Volume 53
Number 9
7 May 2024
Pages 4305–4830

Chem Soc Rev

Chemical Society Reviews

rsc.li/chem-soc-rev

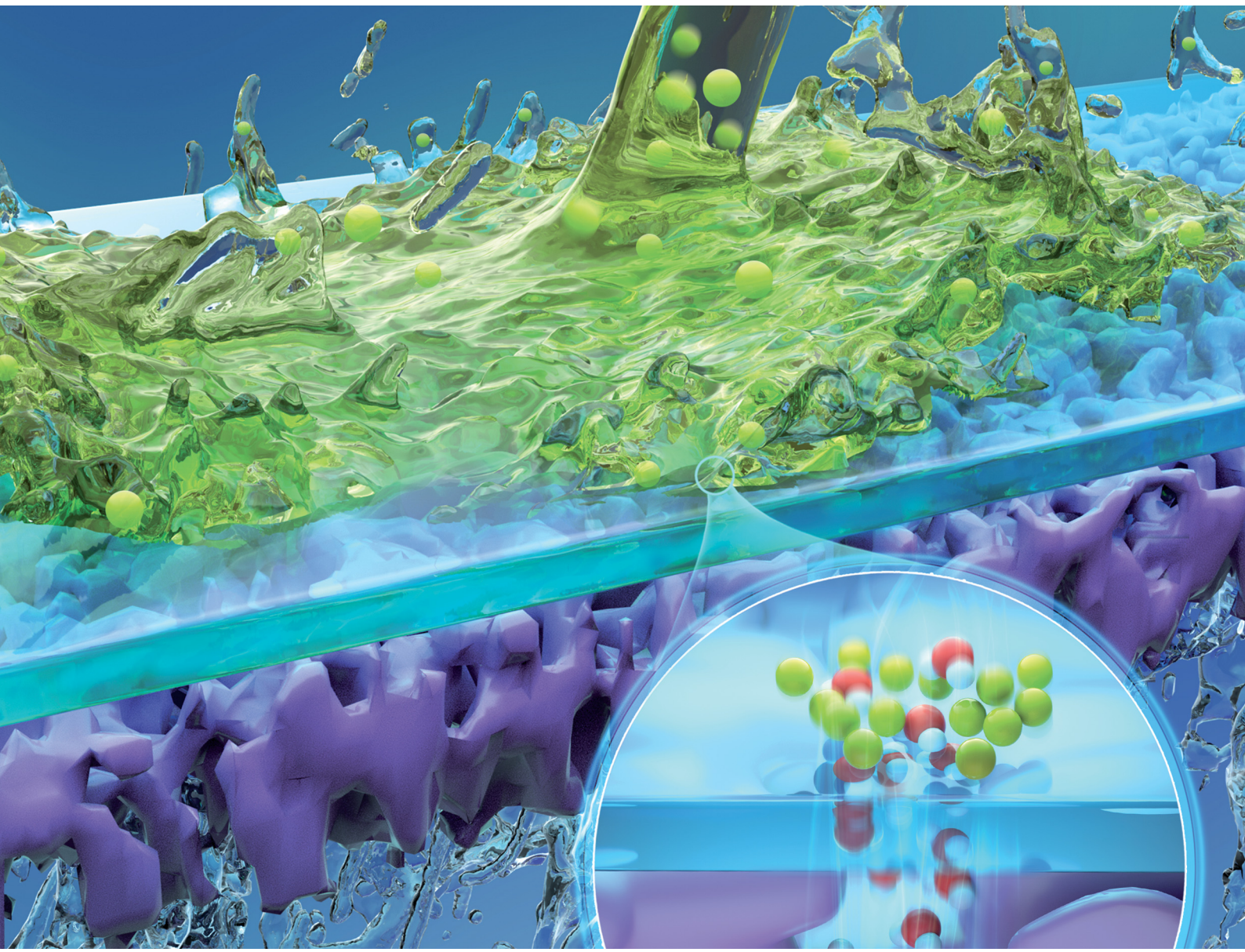

ISSN 0306-0012

ROYAL SOCIETY OF CHEMISTRY

REVIEW ARTICLE

Chuyang Y. Tang *et al.*

Empowering ultrathin polyamide membranes at the water–energy nexus: strategies, limitations, and future perspectives

Chem Soc Rev

REVIEW ARTICLE

View Article Online
View Journal | View Issue

Cite this: *Chem. Soc. Rev.*, 2024, **53**, 4374

Empowering ultrathin polyamide membranes at the water–energy nexus: strategies, limitations, and future perspectives

Pulak Sarkar,[a] Chenyue Wu,[a] Zhe Yang[ab] and Chuyang Y. Tang *[a]

Membrane-based separation is one of the most energy-efficient methods to meet the growing need for a significant amount of fresh water. It is also well-known for its applications in water treatment, desalination, solvent recycling, and environmental remediation. Most typical membranes used for separation-based applications are thin-film composite membranes created using polymers, featuring a top selective layer generated by employing the interfacial polymerization technique at an aqueous–organic interface. In the last decade, various manufacturing techniques have been developed in order to create high-specification membranes. Among them, the creation of ultrathin polyamide membranes has shown enormous potential for achieving a significant increase in the water permeation rate, translating into major energy savings in various applications. However, this great potential of ultrathin membranes is greatly hindered by undesired transport phenomena such as the geometry-induced "funnel effect" arising from the substrate membrane, severely limiting the actual permeation rate. As a result, the separation capability of ultrathin membranes is still not fully unleashed or understood, and a critical assessment of their limitations and potential solutions for future studies is still lacking. Here, we provide a summary of the latest developments in the design of ultrathin polyamide membranes, which have been achieved by controlling the interfacial polymerization process and utilizing a number of novel manufacturing processes for ionic and molecular separations. Next, an overview of the in-depth assessment of their limitations resulting from the substrate membrane, along with potential solutions and future perspectives will be covered in this review.

Received 9th January 2024

DOI: 10.1039/d3cs00803g

rsc.li/chem-soc-rev

[a] *Department of Civil Engineering, The University of Hong Kong, Pokfulam, Hong Kong SAR, China. E-mail: tangc@hku.hk*
[b] *Dow Centre for Sustainable Engineering Innovation, School of Chemical Engineering, The University of Queensland, Brisbane, QLD 4072, Australia*

Pulak Sarkar

Pulak Sarkar is a postdoctoral fellow in environmental engineering working under guidance of Prof. Chuyang Tang at The University of Hong Kong (HKU). He received his BSc and MSc degrees from the University of Kalyani, and his PhD degree in chemical science from the Academy of Scientific and Innovative Research (AcSIR) under the supervision of Dr Santanu Karan in 2022. His research interests focus on the development of high-performance ultrathin reverse osmosis and nanofiltration membranes for ionic and molecular separations.

Chenyue Wu

Chenyue Wu is a PhD student in Environmental Engineering at The University of Hong Kong (HKU) under the supervision of Prof. Chuyang Tang. She received her master's degree in environmental engineering from The University of Hong Kong in 2021. Her current research interests focus on the transport behaviours of polyamide membranes and ion separations using nanofiltration membranes for water treatment.

1. Introduction

A fundamental need for living beings is freshwater. However, as a result of global population expansion, industrial development, and climate change, there is a growing shortage of freshwater all over the world.[1–3] Therefore, an economical and highly energy-efficient water production technology is urgently required to address this shortage.[4] Several distinct types of water purification techniques, like distillation[5] and evaporation[6] have been established for the production of fresh water.[5] Among them, membrane-based water desalination is the most prominent growing technology currently on the market due to the low cost of operation and relatively low energy requirements for the production of freshwater.[7,8]

Thin-film composite (TFC) membranes are the most well-known and widely used membrane categories for water desalination [*e.g.*, reverse osmosis (RO) and nanofiltration (NF)].[9] Generally, the TFC membrane possesses a composite structure, with a top layer that is created *via* interfacial polymerization (IP) on top of the porous ultrafiltration (UF) or microfiltration (MF) substrate, being mainly responsible for the permeation of water/solvents and separation of ions or solutes. Based on literature studies, significant work has been performed to create high-performance TFC membranes for RO or NF applications.[10–12] For example, altering the interfacial kinetics,[13,14] reducing the thickness of the selective layer,[15] post-surface modification,[16,17] introducing various sacrificial interlayers,[18,19] and incorporating various nanostructures within the selective layer[20–22] were all used to improve the membrane separation performance.

Over the past few decades, substantial advancements have been made in the development of a novel type of membrane – ultrathin, highly-permeable TFC membranes, which can significantly reduce energy costs and capital expenditures for water filtration.[10,11,23,24] Among them, membrane thickness plays a crucial role in the transportation of water or solvents, as it is greatly affected by their permeation distance. Therefore, a very thin (or ultrathin) separation layer with a thickness of several nanometers (*e.g.*, ∼ or <10 nm) is ideally perfect for creating a highly permeable TFC membrane while maintaining the separation performance. For example, defect-free polyamide TFC NF membranes with an ultrathin polyamide top layer of <10 nm in thickness, developed *via* the conventional IP method directly on top of a porous substrate, show excellent pure water permeance with a good salt rejection rate.[15,25] A variety of novel fabrication techniques have also been used to create an ultrathin separation layer and its composite membranes. Notable fabrication techniques include controlling the monomer's diffusivity or reactivity at the aqueous–organic interface (*e.g.*, support-free IP,[26,27] vapor-phase IP,[28,29] interlayered-based IP,[30–36] additive-controlled IP,[13,14,37,38] *etc.*) and controlling the volume or concentration of the monomer to control the monomer mass during the IP process (*e.g.*, layer-by-layer assembly,[39–42] spin coating,[43,44] electrospray,[45–48] dual-layer slot coating,[49,50] inkjet printing method,[51–53] *etc.*). These studies reveal how the amount of water transported through polyamide membranes has been significantly altered by an intrinsic or single wall thickness of the top polyamide selective layer.

Despite the potential of the ultrathin separation layer for achieving high water permeance and selective ion transport, its separation capability is yet not fully understood correctly. For instance, some experimental studies have demonstrated that the water permeance of the ultrathin membranes does not necessarily increase with the decrease in thickness of the polyamide separation layer.[54] Indeed, in recent years, numerous studies have shown how the polyamide layer's properties of the composite structure are significantly influenced by the porous substrate, and how the substrate geometry limits the membrane water permeance.[54,55] In addition, generating a defect-free, ultrathin polyamide separation layer on top of a porous substrate is highly challenging. The main drawback of many reported fabrication processes is their inability to produce composite membranes free of defects or pinholes, which, however, is necessary for effective salt sieving. Therefore, there is a critical gap between ultrathin membranes and high-performance membranes, and the challenge lies in achieving a

Zhe Yang

Zhe Yang is an ARC DECRA fellow at the School of Chemical Engineering/Dow Centre for Sustainable Engineering Innovation at the University of Queensland, Brisbane, Australia. He was a Research Assistant Professor in the Department of Civil Engineering at HKU. He received his PhD degree in environmental engineering under the supervision of Prof. Chuyang Tang from HKU. He is recognized as a Top 1% Scholar worldwide ranked by Clarivate Analytics based on citations since 2023. His main research focuses on environment and sustainability using membrane technology in the context of desalination, water reuse, and water/wastewater treatment.

Chuyang Y. Tang

Chuyang Tang is a Chair Professor of Environmental Engineering at The University of Hong Kong. He received his BEng. and MEng. degrees from Nanyang Technological University and PhD degree from Stanford University. His research focuses on membrane synthesis and filter technology, desalination, water reuse, resource recovery, and water-energy nexus. Professor Tang is a Clarivate Highly Cited Researcher. He is a Fellow of the Royal Society of Chemistry and a Fellow of Institution of Civil Engineers. Until now, he has published over 300 refereed publications, with a total citation of more than 30 000 and an H-index of 99 (Web of Science).

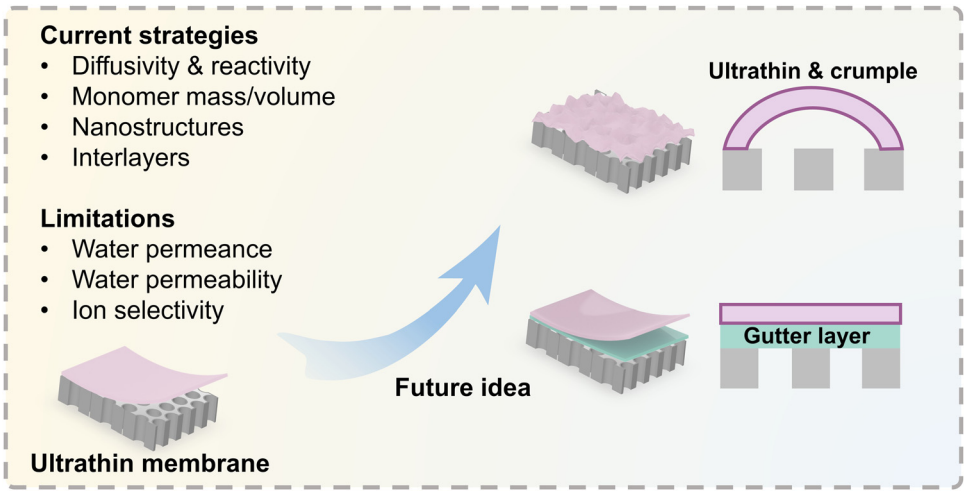

Fig. 1 Illustration of the road map of ultrathin membranes that includes current fabrication strategies, limitations, and future outlooks.

thin polyamide selective layer with a defect-free and well-defined cross-linked structure in order to achieve the desired water permeance and salt rejection.

In this critical review, we highlight cutting-edge fabrication techniques for creating ultrathin polyamide membranes in order to achieve high water/solvent permeance and high salt rejection. We also discuss the limitations and future perspectives of ultrathin polyamide membranes used for ionic and molecular separation (Fig. 1). Although some recent review articles have provided a literature assessment on ultrathin membranes,[56,57] the methods for creating ultrathin membranes have advanced quickly over the past years, so a critical assessment of their limitations and potential solutions for future study is still absent. Therefore, we first unlock the limitations of the ultrathin polyamide selective layer and then discuss some potential strategies to enhance the performance of ultrathin polyamide membranes. Various applications [*e.g.*, organic solvent nanofiltration (OSN), gas separation, carbon capture, pervaporation for the separation of liquid–liquid mixtures, membrane contactors for wastewater treatment, salt–lithium separation, *etc.*] will be discussed to unleash the potential capability of ultrathin membranes. Finally, opportunities for other novel membrane materials (*e.g.*, aquaporins, aligned carbon nanotubes, and graphene-based membranes) will also be highlighted.

2. State-of-the-art strategies and approaches for creating ultrathin polyamide membranes

Interfacial polymerization is a widely recognized polymerization process employed for creating polyamide-based composite membranes. Basically, interfacial polymerization is a reaction–diffusion process that occurs mainly between two highly reactive multi-functional monomers based on the Schotten–Baumann reaction at the liquid–liquid interface between two immiscible solvents.[58–60] The fundamental advantage of this method is that it enables precise control over the development of polymer films, capsules, or fibers for their use in various applications. Utilizing catalysts or initiators could sometimes accelerate the rate of a chemical reaction. The polymerization generally occurs predominantly at the interface between the activators (*e.g.*, monomer A) and the locally available inhibitors (*e.g.*, monomer B) in the organic phase due to the insolubility of inhibitors (*e.g.*, monomer B) in the aqueous phase; as a result of rapid polymerization, a thin polymer film grows at the interface (Fig. 2a). Therefore, with increasing time, the reaction rate slows down and eventually stops due to the increase in the diffusion barrier or thickness of the developed polymer film as the diffusion of monomers in the organic phase is constrained by the polymer thin film that separates the two solutions and the monomers. This suggests that the film thickness created by interfacial polymerization is self-limiting as it grows very quickly at first before slowing down to reach a maximum after some time (Fig. 2a).[61] The top selective layer of TFC membranes is primarily formed through an IP reaction between amine monomers [*e.g.*, piperazine (PIP) for semi-aromatic polyamide structure and *m*-phenylenediamine (MPD) for fully-aromatic polyamide structure] and acyl chloride monomers [*e.g.*, trimesoyl chloride (TMC)] at the aqueous–organic interface on top of a porous substrate [*e.g.*, polyacrylonitrile (PAN), polysulfone (PSf), polyether sulfone (PES), *etc.*] (Fig. 2b).[13,15] Since the IP reaction is a diffusion-limited process, highly reactive monomers initially form a dense thin layer that results in a thinner film compared to less reactive monomers. As an example, the MPD-TMC film (with an intrinsic thickness of ~20 nm) is thinner than the PIP-TMC film (thickness of ~100 nm) as MPD monomers are more reactive to TMC than PIP monomers.[62] However, several parameters influence the morphology and thickness of the generated polymer films during the polymerization process such as solubility,[63] concentration,[64] reactivity,[65] structure,[66–69] and stoichiometry[60,70,71] of the monomers, the solvent media and temperature,[72,73] the diffusivity of the monomers,[74] additives,[75] post-treatment after IP,[15] *etc.* In the literature, a variety of fabrication techniques have been employed to develop high-performance ultrathin polyamide membranes by regulating these parameters.

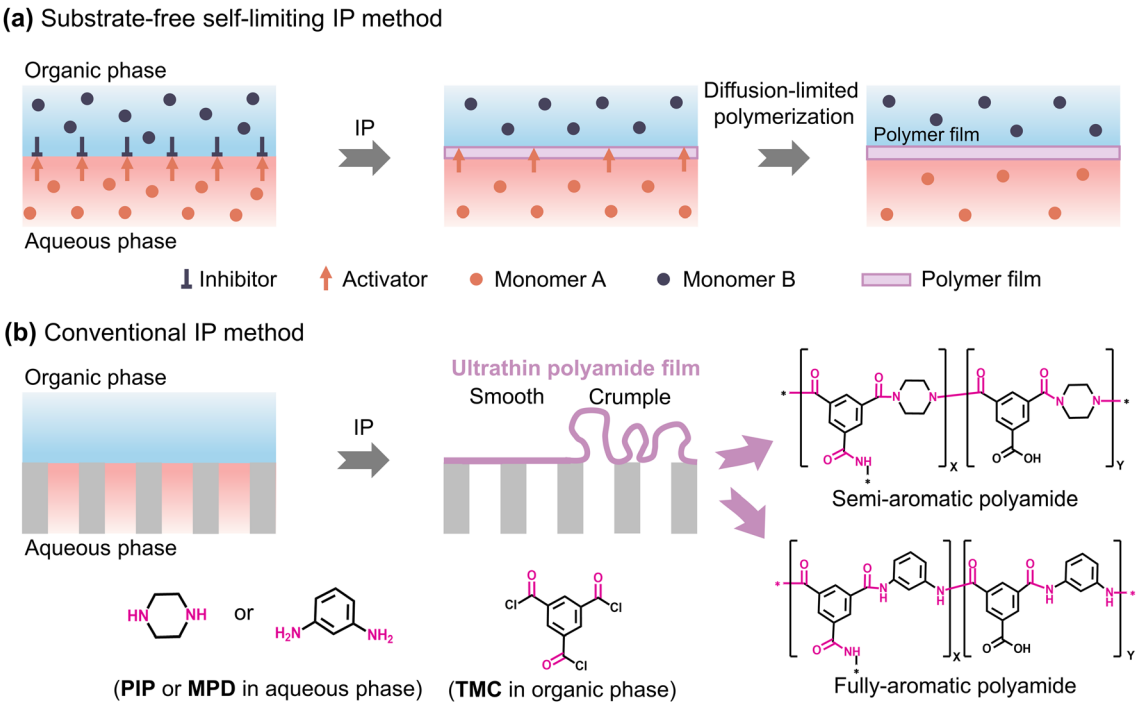

Fig. 2 Schematic presentation of the (a) substrate-free interfacial polymerization (IP) method to form a self-limiting polymer film at the free aqueous–organic interface and (b) conventional interfacial polymerization (IP) method to fabricate polyamide TFC membranes. PIP: piperazine; MPD: *m*-phenylenediamine; and TMC: trimesoyl chloride.

The following discussion covers the details of the state-of-the-art strategies for constructing ultrathin polyamide membranes.

2.1. Regulation of volume or concentration of the monomers for fabricating ultrathin polyamide membranes

The concentration and volume or mass of the reacting monomers are the key factors in controlling the thickness of the top polyamide selective layer. In most fabrication techniques, the regulation of monomer concentration from low to high has been extensively used to create ultrathin membranes (Table 1).[18,25] Since reducing the volume or mass of the monomers is crucial for cutting down the overall manufacturing cost for large-scale fabrication processes, recent studies concentrated on finding ways to regulate the volume or mass of the monomers used to create ultrathin membranes while maintaining the separation performance. In the following sections, some specific fabrication techniques utilized to regulate the volume or mass of the monomers for the fabrication of ultrathin membranes are covered.

2.1.1 Fabrication of ultrathin membranes *via* layer-by-layer (LbL) assembly or the dip-coating method. Layer-by-layer (LbL) assembly-based thin films have garnered a lot of attention in recent years due to their ability to create controllable film thickness at the nanometer level and their wide range of material opportunities.[76,77] The LbL assembly of thin films can be formed utilizing a variety of techniques such as dipping,[78] spinning,[79] roll to roll,[76] atomization,[80] electrochemical deposition,[76] *etc.* The most widespread approach for creating thin films and their composite structure is LbL assembly using the dip-coating technique, which was invented by Decher for creating polymer multi-composites in 1997.[81] In this method, a substrate is manually dipped into different solutions with desired materials and then rinsed with particular electrolyte solutions to form a thin film.[82,83] Many researchers employed the molecular LbL assembly technique to fabricate TFC membranes.[39–42,84] To fabricate ultrathin organic network-based NF membranes, the solution-based LbL assembly method was first adopted in the year 2012.[39] In this process, the growth of polyamide films has occurred *via* polymerization between tetraphenylmethane-4,4′,4″,4‴-tetraacyl chloride (TPMC) and tetrakis(4-aminophenyl)-methane diamine (TAPM) monomers.[39] The NF membranes produced using this method display superior separation efficiency in terms of both water permeance and bivalent salt rejection (*e.g.*, Na_2SO_4) (Table 1).[39] Polyamide-based TFC RO membranes were also created *via* the molecular LbL (mLbL) assembly method utilizing MPD and TMC monomers on top of the PAN substrate for water desalination (Fig. 3a).[40] The fabricated membrane enables the controlled creation of a defect-free ultrathin polyamide layer with very low surface roughness (Table 1 and Fig. 3b).[40] The membrane also shows excellent separation performance and good antifouling properties compared to the conventional TFC RO membranes (Table 1).[40] Later in 2015, polyamide-based desalination membranes were developed by using the mLbL method by dipping in various monomer solutions to regulate the selective layer thickness (ranging from 10 to 13 nm) and surface roughness more accurately (Fig. 3c).[41] Additionally, the mLbL-assembled membranes exhibit very good separation performance in terms of water flux which is 2.5 times

Table 1 Summary of ultrathin polyamide NF and RO membranes

Fabrication method	Membrane	Material used	Separation performance			Ref.
			Permeance [L m^{-2} h^{-1} bar^{-1}]	Rejection [%]	PA layer thickness [nm]	
Nanofiltration (NF) membranes						
Conventional IP	Ultrathin polyamide films	PIP/TMC	46.6 for water	98.1 for Na_2SO_4	8.5	25
IP followed by post-treatment	Sub-5 nm polyamide nanofilms	PIP/TMC	61.3 for water	99.5 for Na_2SO_4	4.6	15
Molecular layer-by-layer (mLbL)	Ultrathin films of organic networks	TPMC/TAPM	17.8 for water	87.4 for Na_2SO_4	16.6	39
	Ultrathin microporous polyamide films	TAPB/TMC	8.4 for ethanol	86.0 for methyl orange	17	42
Spin coating	Spin-assisted GO–polyamide membranes	GO-PIP/TMC	35.1 for water	93.6 for Na_2SO_4	20	89
	Spin-coating assisted ultrathin membranes	PIP/TMC	36.1 for water	96.2 for Na_2SO_4	9.7	43
Electrospray	Ultrathin polyamide membranes	MPD/TMC	11.1 for water	57.0 for Na_2SO_4	10.8	45
	Polyamide membranes with hierarchical nanostructures	PEI/TMC	23.7 for water	>95 for brilliant blue	13.8	48
Support-free IP	Nanofilm composite membranes	PDA-PIP/TMC	25.1 for water	99.1 for Na_2SO_4	12	103
Vacuum-assisted IP	Polyamide membranes *via* vacuum-assisted IP	PIP/TMC	20 for water	99.6 for Na_2SO_4	19.2	114
Diffusion-controlled IP	Turing type polyamide membranes	PVA-PIP/TMC	26.0 for water	99.6 for Na_2SO_4	~20	117
	Ultraselective polyamide membranes	SLS-PIP/TMC	23.1 for water	99.95 for Na_2SO_4	~12	13
	Ultra-permselective NF membranes	PCS-PIP/TMC	44.7 for water	98.0 for Na_2SO_4	14	37
	MONs assisted NF membranes	MONs-PIP/TMC	41.7 for water	98.0 for Na_2SO_4	15	20
Interlayered IP	SWCNT film supported NF membranes	PD/SWCNTs-PIP/TMC	32.0 for water	95.9 for Na_2SO_4	12	30
	SWCNTs supported membranes	SWCNT-PIP/TMC	40 for water	96.5 for Na_2SO_4	15	34
	COF supported polyamide membranes	COF-PIP/TMC	31.1 for water	95.0 for Na_2SO_4	20	36
	Ultrathin TFC polyamide membranes	PVA-PIP/TMC	31.4 for water	99.4 for Na_2SO_4	9.6	133
In situ free IP	Ultrathin film composite membranes	PIP/TMC	26.6 for water	98.7 for Na_2SO_4	13.4	54
Reverse osmosis (RO) membranes						
Molecular layer-by-layer (mLbL)	TFC RO membranes	MPD/TMC	1.4 for water	95.7 for NaCl	20	40
	Tailor-made polyamide membranes	PEI/PAA-MPD/TMC	1.5 for water	98.2 for NaCl	25	41
Dual-layer slot coating	TFC RO membranes	MPD/TMC	2.1 for water	99.1 for NaCl	8.8	49
	Interfacial adhesion tailored TFC RO membranes	PDA-MPD/TMC	2.6 for water	99.5 for NaCl	7.2	50
Vapor phase IP	TFC membranes without using organic solvents	MPD/TMC	3.3 for water	94.3 for acridine orange	12.4	28
Support-free IP	TFC RO membranes *via* support-free IP	MPD/TMC	0.9 for water	99.0 for NaCl	17.1	27
	Ultrathin polyamide nanofilms for RO	MPD/TMC	2.69 for water	96.0 for NaCl	6.5	26
Vacuum-assisted IP	TFC RO membranes *via* vacuum-assisted MPD loading	MPD/TMC	2.8 for water	98.7 for NaCl	16.6	115
Interlayered IP	Sub-10 nm polyamide nanofilms	MPD/TMC	3.1 for methanol	99.7 for methyl orange	8.4	18
Dual-layer IP strategy	Asymmetrical ultrathin polyamide membranes	PIP/TMC – MPD/TMC	2.86 for water	97.3 for NaCl	13	173
In situ free IP	Ultrathin film composite membranes	MPD/TMC	2.9 for water	98.3 for NaCl	6.7	54

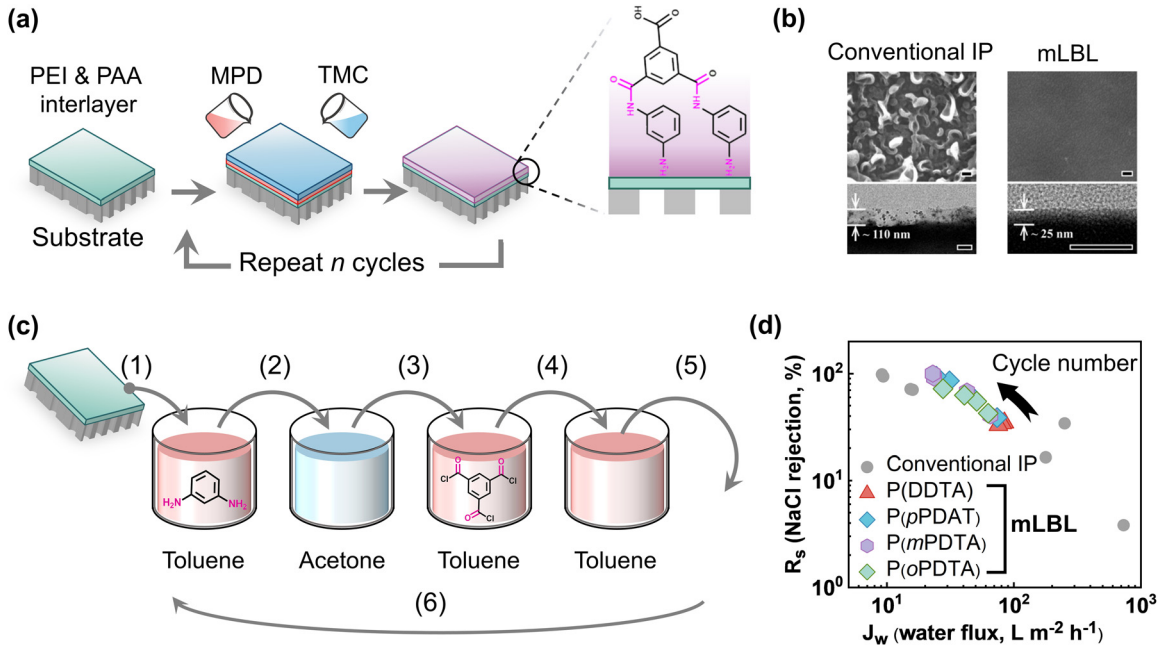

Fig. 3 (a) Strategies for creating polyamide TFC membranes *via* mLbL assembly method, and (b) the control of surface morphology from crumpled to smooth with desired thickness using the mLbL assembly method (scale bar is 100 nm for all SEM and TEM images). Scanning electron microscopy and transmission electron microscopy images are reproduced with permission from ref. 40, Copyright 2013, WILEY-VCH. (c) Fabrication of polyamide TFC membranes using the mLbL method by dipping in various monomer solutions. (d) The figure presenting the NaCl rejection *vs.* water flux of the prepared TFC membranes. These values are adapted from ref. 41.

higher compared to conventional IP-based membranes, and NaCl rejection (up to 98.2%) (Table 1 and Fig. 3d).[41] In 2021, the dip-coating-based mLbL deposition method was also utilized to create high-performance TFC membranes for organic solvent nanofiltration (OSN) applications.[42] The layer-by-layer dip-coating technique describes how 1,3,5-tris(4-aminophenyl)benzene (TAPB) and trimesoyl chloride (TMC) can react to create highly cross-linked defect-free ultrathin polyamide separation layers.[42] The fabricated ultrathin (thickness ~17 nm) membranes maintained a high rejection rate of methyl orange (~86.0%) while demonstrating outstanding solvent permeance (*e.g.*, ethanol, dimethylformamide, methanol, and acetonitrile) (Table 1).[42] Overall, this mLbL assembly through the dip-coating approach has demonstrated wide applicability in the design of high-performance ultrathin polyamide-based TFC membranes with controlled top layer thickness, roughness, and separation properties.

2.1.2 Fabrication of ultrathin membranes *via* spin-coating method. A widely employed technique called spin coating has been utilized to create highly oriented/polycrystalline thin films, polymer nanofibers, and patterned thin films.[85–87] Compared to other coating processes, spin-coating technology generally produces more homogeneous and well-organized films, making it a particularly helpful method for creating transparent films and optical coatings with customizable and uniform colors.[76] Generally, in this method, a casting/aqueous/organic monomer solution is either applied to a spinning substrate or to a static substrate followed by spinning at a particular rotation speed (Fig. 4a). Many forces, including electrostatic forces, centrifugal forces, air shear, and viscous forces, play important roles in the spin-coating procedure compared to the traditional immersion-based coating process. The spin speed and thickness of the spin-coated film are closely correlated, where higher spin speeds result in thinner films. As a result, the thickness of the polymer films could be controlled or tailored by regulating the spin speed (Fig. 4a).[88] Additionally, the spin-coated films display significantly lower roughness than those made using other approaches. One of the primary drawbacks of the spin-coating process is the production of a small membrane area since it requires faster spin rates to create a membrane on top of a large substrate. However, the benefits of implementing the spin-coating method for creating ultrathin films make it a great option for membrane research and development. As an example, the graphene oxide–polyamide composite NF membrane was fabricated *via* the spin-assisted IP strategy while the centrifugal force generated by spin could successfully create ultrathin (thickness ~20 nm) and defect-free polyamide membranes (Table 1).[89] The resulting GO–polyamide composite membranes exhibit an excellent water permeance of 35.1 L m^{-2} h^{-1} bar^{-1} while maintaining moderate rejection of Na_2SO_4 (up to 93.6%) (Table 1).[89] Additionally, the GO–polyamide composite membranes display exceptional durability under harsh conditions and chemicals.[89] In the year 2022, using the spin-coating assisted IP method, a 9.7 nm thick ultrathin polyamide nanofilm, and its composite membranes were reported to be formed on top of the PSf substrate by regulating the rotation speed, spinning volume, and concentration of amine monomers (Table 1 and Fig. 4a).[43] The resulting membrane exhibits high water permeance (up to 36.1 L m^{-2} h^{-1} bar^{-1})

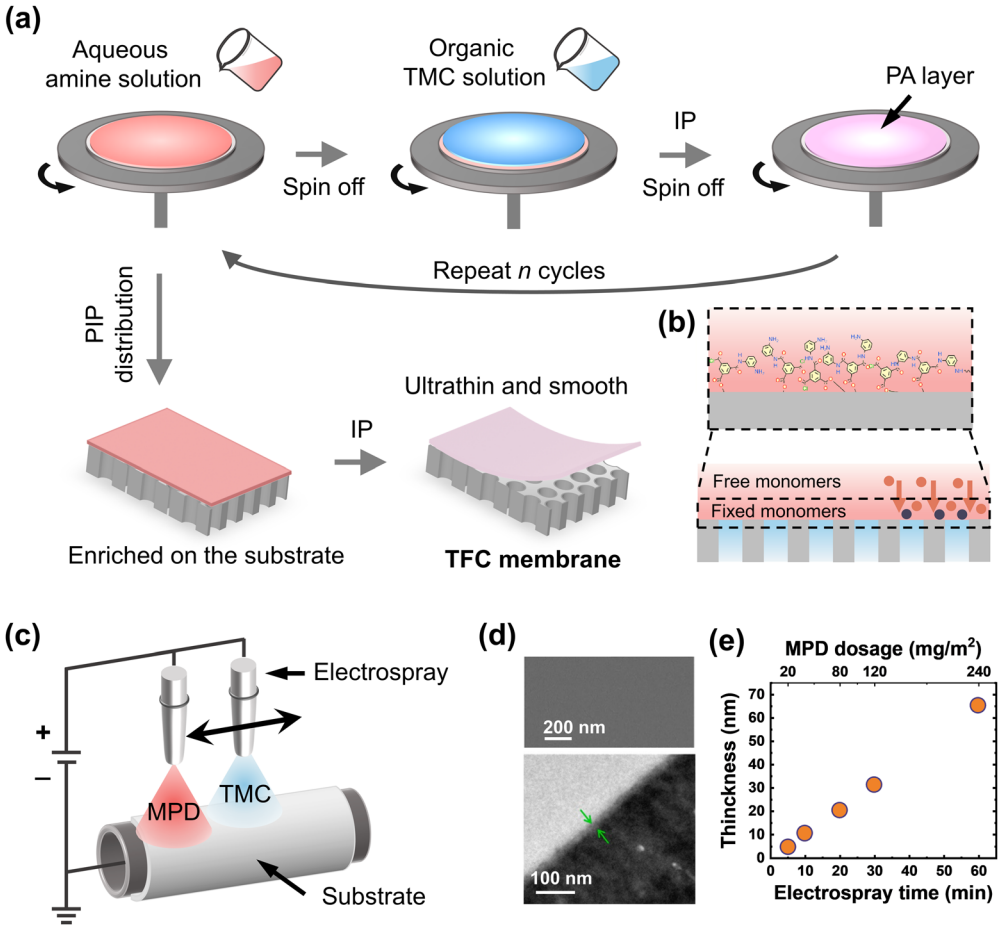

Fig. 4 (a) Step-by-step fabrication of polyamide thin film composite membranes *via* the spin-coating assisted IP method on top of porous substrate. (b) A possible mechanism of how spin-coating helps in reducing the diffusion of the monomers and making a stable reaction zone during the film formation. (c) An illustration of the electrospray method from the side and from the top and (d) SEM and TEM images of the polyamide membranes. Scanning electron microscopy and transmission electron microscopy images are reproduced with permission from ref. 45, Copyright 2018, American Chemical Society. (e) Thickness variation of the fabricated polyamide membranes with different electrospraying times and MPD dosages. These values are adapted from ref. 45.

as well as moderate rejection of Na_2SO_4 (up to 96.2%) (Table 1).[43] Indeed, the physicochemical properties such as surface morphology, roughness, thickness, and the degree of network cross-linking of the top selective layer of the polyamide TFC membranes can be accurately adjusted by altering the monomer ratios and deposition cycles using the spin-assisted layer-by-layer deposition method as the IP reaction happened at the stable solid–liquid interface (Fig. 4b).[44]

2.1.3 Fabrication of ultrathin membranes *via* electrospray method. Electrohydrodynamic spraying, which is also known as electrospraying, is a technique used for atomizing liquids using electrical forces.[90] It is a widely used and efficient method for electroscrubbing, thin-film manufacturing, surface coating, *etc.*[90] In this technique, the electric field causes the liquid to flow out of a capillary nozzle, which is maintained at a high electric potential, and compels it to disperse into tiny droplets (Fig. 4c). This method has the added advantage that droplet size and droplet production can be regulated by manipulating the liquid's flow rate and electric potential. This technique has recently been used widely by researchers to create ultrathin polyamide TFC membranes.[45–48] In 2018, the electrospray-assisted IP process was first introduced to fabricate ultrathin polyamide RO membranes with a controlled top layer thickness where the polymerization reaction occurs at the interface between the fine microdroplets of MPD and TMC monomers. (Fig. 4c).[45] The method demonstrates that, in contrast to the ridge-and-valley structure produced using the traditional approach, electrospray-assisted IP creates much smoother structures of polyamide membranes (Fig. 4d).[45] With a linear growth rate of roughly 1 nm per minute, the polyamide layer's thickness can also be controlled between 4 nm and 100 nm (Table 1 and Fig. 4e).[45] The resulting membranes displayed three times higher pure water permeance in comparison to membranes created using the traditional IP process. Overall, their research provides a novel approach for designing and creating ultrathin polyamide RO membranes with tunable separation performance.[45] In the same year, the fabrication of ultrathin polyamide TFC RO membranes was reported by using the electrospraying process for desalination applications (Fig. 4c).[46] The prepared membranes using this process show much smoother and thinner polyamide films in comparison with state-of-the-art fabrication techniques. The method shows

that the thickness of the polyamide films can be reduced to as thin as 15 nm with a 4 nm increase in each scan while maintaining the desalination performance.[46] Later, the electrostatic atomization-aided IP technique was used to create polyamide membranes with hierarchical nanostructures.[48] Using this technique, the membrane nanostructure and the top layer thickness can be accurately adjusted by altering the amount of monomer and the monomer ratio.[48] This technique results in an ultrathin polyamide layer that retains the ability to reject brilliant blue dye while exhibiting ultrafast solvent permeance (*e.g.*, 23.7 L m^{-2} h^{-1} bar^{-1} for water, 39.5 L m^{-2} h^{-1} bar^{-1} for methanol, and 56.9 L m^{-2} h^{-1} bar^{-1} for acetone) (Table 1).[48] In terms of permeance-rejection behavior, the membranes surpass the upper limit of the reported TFC membranes.[48] Overall, the controllable advantage of the electrospray process provides strong motivation for the creation of novel materials and offers an innovative method for making the next-generation ultrathin polyamide TFC membranes.

2.1.4 Fabrication of ultrathin membranes *via* an inkjet printing method. The inkjet printing process has also been extensively used to create different types of membranes, similar to the other fabrication techniques.[91–93] This technique offers a quick and straightforward fabrication approach and results in homogeneous deposition of the monomer with regulated volume or mass and therefore generates very low chemical waste.[51,91–93] Fabrication of TFC RO membranes using the inkjet printing method was first introduced by Arnusch and co-workers[51,92] in the year 2015. In this method, a polyamide selective layer was created on top of the porous substrate by employing an aqueous MPD solution as an ink, followed by interfacial polymerization to react with TMC without using any draining procedures.[51] According to the findings, increasing the coating layers on the porous substrate leads to an increase in the degree of cross-linking, membrane thickness, and hydrophilicity of the membranes. The fabricated membrane exhibits comparable separation performance to the membrane created using other techniques.[51] Inkjet printing was also utilized to produce organic solvent nanofiltration (OSN) membranes by using polyethyleneimine (PEI), single-walled carbon nanotubes (SWCNT), and TMC on top of a porous polyketone (PK) substrate.[52] The inkjet printing technique generates polyamide membranes with a top active layer thickness as thin as 151.6 nm and exhibits good separation performance in different organic solvents with high rejection of dyes.[52] Later, the fabrication of a polyamide TFC membrane was reported by inkjet printing aqueous MPD ink and organic TMC ink onto a porous PVDF substrate.[53] The method demonstrated that a defect-free and dense polyamide selective layer can be successfully produced by controlling the coating of aqueous and organic solutions while using a minimal amount of monomers. Therefore, the inkjet printing process offers an advanced manufacturing technique for the creation of next-generation polyamide TFC membranes. However, according to data from the literature, in order to enhance water permeability, the top polyamide layer needs to be extremely thin (below 20 nm) which is quite challenging and appears to be this method's biggest disadvantage. These limitations can be resolved in the future by properly implementing this inkjet printing strategy.

2.1.5 Fabrication of ultrathin membranes *via* dual-layer slot coating (DSC) method. The dual-layer slot coating (DSC)

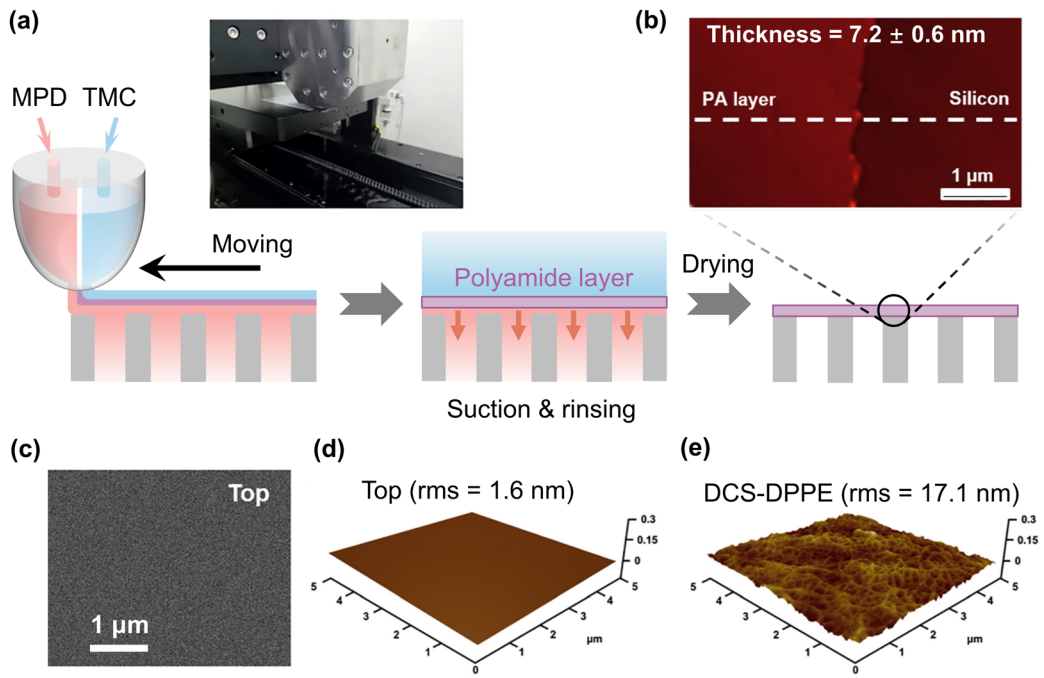

Fig. 5 (a) Schematic view of the fabrication of polyamide membranes *via* the dual-layer slot coating method. (b) Cross-sectional AFM image of the polyamide layer on top of the silicon wafer surface. (c) SEM surface morphology, (d) AFM surface morphology, and (e) surface root-mean-square-roughness (rms) of the fabricated polyamide layer using the DSC method. Reproduced with permission from ref. 50, Copyright 2020, Elsevier B.V.

method has recently been the topic of numerous research studies, which addressed several critical issues such as operating cost, process effectiveness, and less energy consumption.[94–96] The DSC method is a highly effective coating process used to produce dual-layer thin films. The DSC method involves the simultaneous deposition of two different monomer solutions, unlike the traditional IP method, which applies monomer solutions one at a time. This creates a polyamide film, which is then eventually deposited onto a moving substrate to create a TFC membrane. As a result, by reducing the number of fabrication steps, the DSC approach may make it feasible to produce TFC membranes at reduced costs. Also, as the polyamide film is formed at the free interface between two monomer solutions, its structure remains uninfluenced by the characteristics of porous substrates. As a result, this method helps to enable a more accurate understanding of both the structure–property–performance relationship of the TFC membranes and the mechanism of the development of polyamide films at the interface. In the year 2017, the DSC method was first introduced to fabricate polyamide TFC RO membranes by using *in situ* polymerization between MPD and TMC monomers followed by transferring them onto different porous substrates (Fig. 5a).[49,50] The interfacial adhesion between the polyamide film and the substrate is also employed to modify the substrate using an O_2 plasma treatment and/or a polydopamine coating, which helps to further reduce the thickness of the polyamide film.[50] This DSC approach produces an extremely thin polyamide layer (thickness as low as 7 nm), a very smooth polyamide structure, and less negatively charged surfaces on top of the modified substrate compared to the conventional IP process (Table 1 and Fig. 5b–e). Additionally, the membrane fabricated using this method exhibits very good water permeability and high rejection of NaCl compared to conventional IP-based TFC RO membranes.[49,50] Therefore, the DSC process offers a simple and adaptable way to make ultrathin polyamide TFC membranes with exceptional separation performance.

2.1.6 Vapor phase interfacial polymerization (IP) for creating ultrathin membranes. A growing and effective method for creating covalent organic frameworks (COF) membranes or polymer-based TFC membranes with an ultrathin separation layer is the vapor phase IP strategy.[28,97–99] In this approach, interfacial polymerization takes place at the aqueous–vapor interface. In contrast to the traditional IP method, where IP is performed at the aqueous–organic interface, the vapor phase IP method is more eco-friendly since this approach does not require any organic solvent; therefore it is more economical and less harmful to the environment. The vapor phase IP strategy was first reported in the year 2021, to create a polyamide-based TFC RO membrane with an ultrathin separation layer (thickness $\sim$12.4 nm) for the removal of micropollutants from water which enables a high water permeance of up to 3.3 L m^{-2} h^{-1} bar^{-1} (Table 1).[28] This technique can successfully regulate the surface morphology, degree of crosslinking, and even the top selective layer thickness by altering the applied temperature and the synthesis time.[28] Later in 2022, polyester–polyamide-based TFC membranes were fabricated *via* the vapor phase IP reaction between the vapor of TMC, and an aqueous solution containing β-cyclodextrin (β-CD) and PIP monomers.[29] In comparison to commercial membranes, the produced membranes exhibit one order of magnitude higher permeance and superior separation performance in aqueous, organic, and aqueous–organic mixture systems.[29] As a result, the vapor phase IP method is an attractive approach for fabricating ultrathin membranes with customizable separation performance for their use in RO/NF applications.

Several different approaches for creating ultrathin membranes have been reported in the literature that are similar to the vapor phase IP method. For example, diamond-like carbon (DLC) membranes have been created using the chemical vapor deposition (CVD) process since the early 1990s.[100,101] In 2012, a parallel-plate plasma-enhanced CVD reactor was employed to develop ultrathin freestanding DLC membranes.[102] The fabricated membranes exhibit extremely high mechanical strength and excellent stability in organic solvents since sp^3 carbon networks are present within the structure.[102] As a result, the CVD approach provides an effective method for producing membranes with adjustable thickness. In the future, high-performance ultrathin membranes can be developed *via* the layer-by-layer (LbL) CVD process to tune the membrane properties for their use in ionic and molecular separation applications.

2.2. Controlling the diffusivity/reactivity of the monomers at the aqueous–organic interface

2.2.1 Support-free interfacial polymerization to create ultrathin membranes. In this technique known as support-free interfacial polymerization, the reaction takes place directly at the aqueous–organic interface, unlike the conventional fabrication approach where the IP reaction occurs on the top of porous substrates. However, monomer diffusion at the free interface significantly influences the growth of the polyamide film. The limitations of the traditional IP method have been overcome by this support-free IP method.[26,27,103] It enables the creation of high-performing TFC membranes by employing an ultrathin polyamide selective layer in a straightforward yet controllable method. For example, in 2017, the support-free IP method was utilized to produce polyamide-based TFC RO membranes.[27] In contrast to the conventional method, the support-free IP method successfully produced an ultrathin and smooth polyamide film with a less negatively charged surface due to the uniform monomer diffusion at the support-free interface during film formation (Table 1).[27] Additionally, the prepared membranes using this method display good perm-selectivity due to the self-healing of the nanosized defects in the rejection layer.[27] In 2018, smooth ultrathin sub-8 nm polyamide nanofilms were reported *via* the support-free IP method at the aqueous–organic interface (Table 1 and Fig. 6a–d).[26] The resulting membrane exhibits four times greater water permeance than conventional composite membranes.[26] Therefore, the support-free IP method is indeed a useful method for fabricating ultrathin polyamide membranes by controlling the diffusivity of the monomers at the interface.

2.2.2 Fabrication of ultrathin membranes *via* the vacuum-assisted method for homogeneous distribution of monomers.

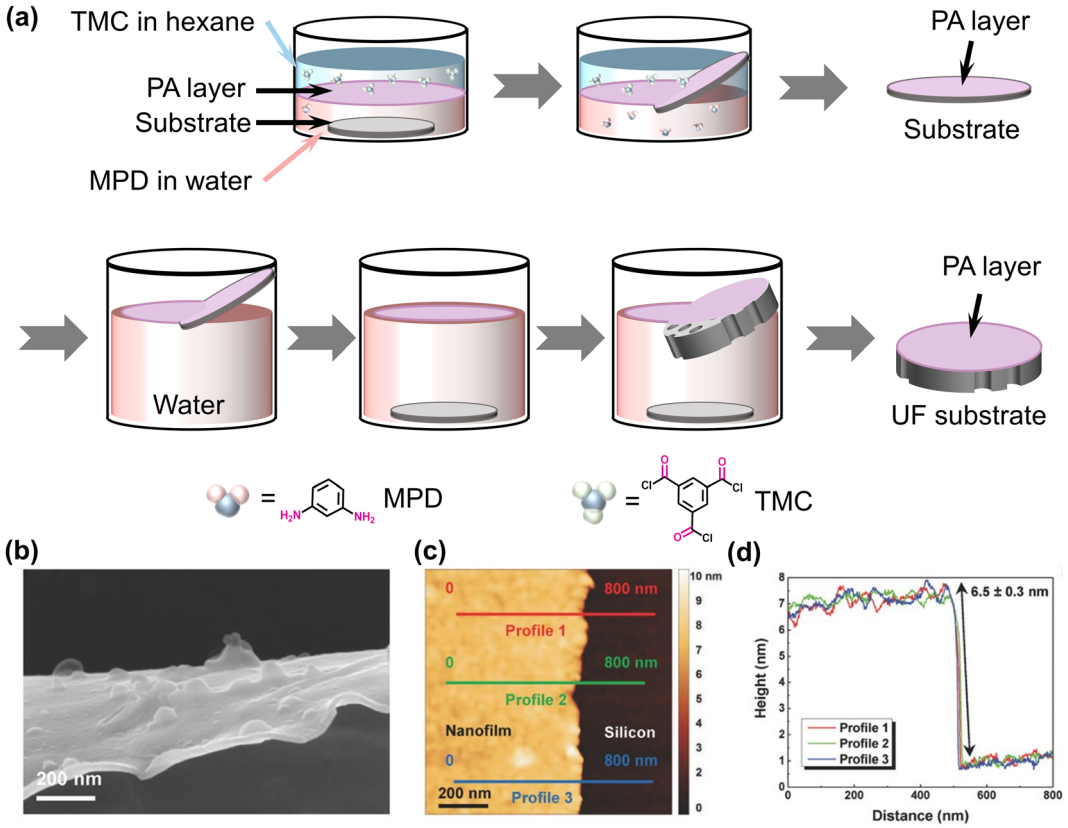

Fig. 6 (a) Step-by-step schematic presentation of freestanding polyamide film created at the free aqueous–organic interface followed by transferring onto porous substrates. (b) SEM cross-sectional image of the freestanding polyamide film, and (c) and (d) cross-sectional AFM image along with the height profile of the polyamide film on top of the silicon wafer. Reproduced with permission from ref. 26, Copyright 2018, Wiley-VCH.

In the middle of the 19th century, vacuum filtration was first implemented for industrial filtration applications.[104] In recent years, this method has gained significant acceptance within the scientific community. Despite having a filtration-related use, this technique also holds potential for coating various nanomaterials such as nanowires,[105] nanosheets,[106–109] nanoparticles,[110] *etc.* on top of the specified substrates. This approach has subsequently been used for the manufacture of TFC RO/NF membranes. By employing this vacuum-assisted technique, various interlayered-based membranes were designed to improve the separation performance of the TFC membranes. As an example, between the polyamide selective layer and the porous UF substrate, GO nanosheets,[111] nanocrystals,[112] covalent organic frameworks (COF)/metal–organic frameworks (MOFs),[19,36,113] nanostrand layers,[18] MWCNT,[30] nanorods,[20] *etc.* were introduced. However, this technique was also used to create TFC membranes *via* interfacial polymerization in order to enhance the distribution of amine monomers on top of the porous substrate.[114–116] For example, polyamide-based TFC membranes were fabricated using the vacuum-assisted technique to increase the homogeneity of the distribution of the amine monomers on top porous substrates.[114] The method demonstrates that the homogeneous and uniform distribution of amine monomers promotes the IP reaction between PIP and TMC to create a defect-free ultrathin polyamide separation layer with a thickness below 20 nm (Table 1). The membrane also shows homogeneous surface features with roughness below 20 nm while maintaining a significant cross-linked network structure. The produced membrane displays a high water permeability of up to 20 L m^{-2} h^{-1} bar^{-1} with a high rejection of Na_2SO_4 of up to 99.6% (Table 1).[114] A polyamide-based RO membrane with ridge and valley morphology of the polyamide top layer on top of a porous substrate was created by employing vacuum-assisted MPD loading.[115] This technique significantly increased the availability of amine monomers during the IP reaction, thus enhancing the ridge and valley structure of the top polyamide separation layer. The constructed ultrathin membranes showed an excellent water permeance of up to 2.8 L m^{-2} h^{-1} bar^{-1} while maintaining a high rejection of NaCl of up to 98.7% (Table 1).[115] Therefore, the vacuum-assisted IP technique is a successful strategy for fabricating ultrathin polyamide membranes to control the top layer thickness, surface morphology, and separation performance.

2.2.3 Introducing different organic molecules/polymers to control the diffusion of monomers. An intriguing technique for creating ultrathin and defect-free polyamide TFC membranes is to control the monomer diffusion at the aqueous–organic interface. Together with the monomers, various compounds/chemicals can be added into the aqueous and organic phases in order to successfully control the diffusion of the reacting

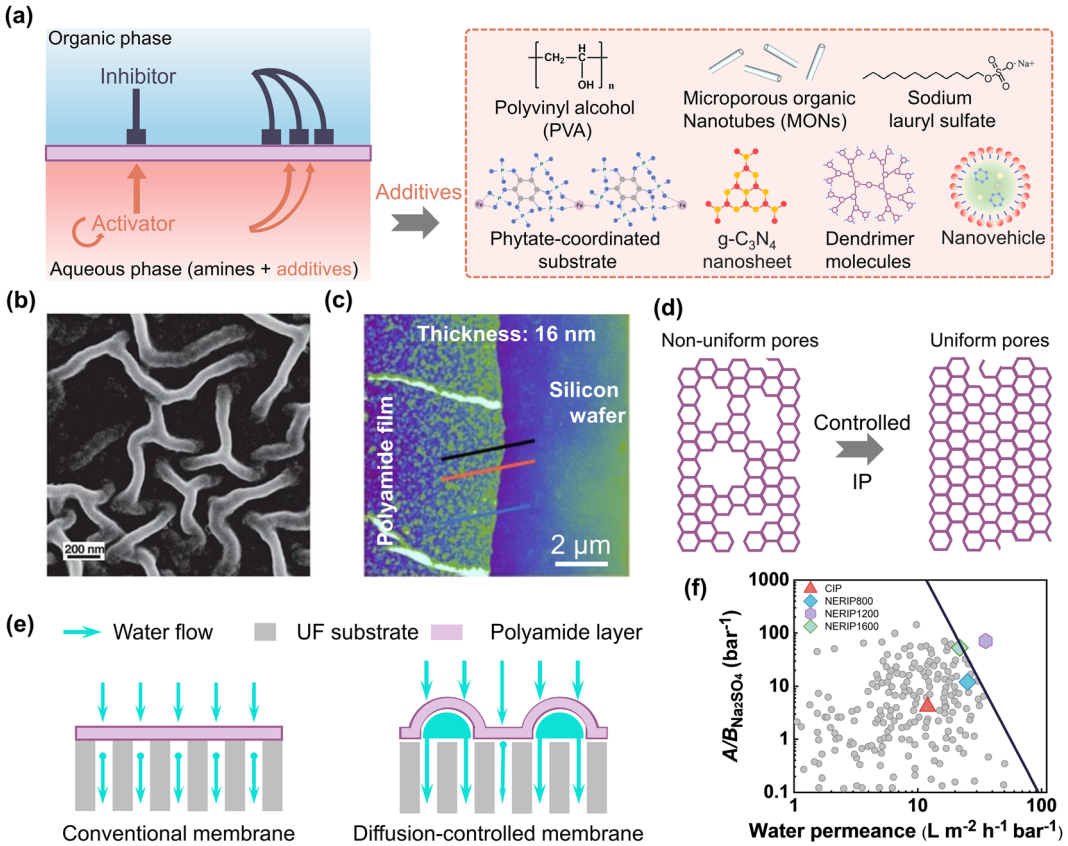

Fig. 7 (a) A schematic representation of the diffusion-controlled IP method that uses different additives to produce polyamide membranes during IP. (b) SEM images of the crumpled membranes produced by the diffusion-controlled IP technique. Reproduced with permission from ref. 117, Copyright 2018, American Association for the Advancement of Science. (c) AFM cross-sectional images of the ultrathin polyamide nanofilms formed with diffusion-controlled IP method. Reproduced with permission from ref. 20, Copyright 2022, Springer Nature. (d) A schematic representation of the polyamide network structure showing the uniformly produced pore size distribution in the presence of additives. (e) A schematic representation of the transport of water across the smooth and wrinkled membranes that are created in the presence of additives. (f) An overview of the water/Na_2SO_4 selectivity and water permeance of the state-of-the-art NF membranes as reported in the literature. These values are adapted from ref. 22.

monomers during interfacial polymerization. As an example, various organic molecules or polymers (*e.g.*, polyvinyl alcohol (PVA),[117] *o*-hydroxy porous organic polymers (*o*-POPs),[118] dendrimers,[119] *etc.*) were added to the aqueous/organic solution along with the monomers. Based on literature reports, the thickness of the polyamide film can vary depending on how quickly the monomers diffuse at the reaction interface (Fig. 7a). In addition, the rate at which the monomers diffuse at the interface has a considerable effect on the surface morphology (smooth or crumpled) of the generated polyamide film. For example, a nanoscale "Turing" type morphology of the polyamide membranes was created by employing PVA macromolecules in the aqueous solution with the PIP monomers (Fig. 7a).[117] The addition of PVA macromolecules facilitates hydrogen bonding with the PIP monomers and raises the solution's viscosity, which hinders the PIP monomers from diffusing into the organic phase and results in the generation of nanoscale spotted and striped structures (*i.e.*, Turing patterns) due to the diffusion-driven instability at the interface (Fig. 7b). Therefore, the effective surface area of the fabricated membranes increases, considerably enhancing water permeability and water–salt separation performance, surpassing the upper-bound line of cutting-edge NF membranes (Table 1).[117] Thin film nanocomposite (TFN) membranes were also created using the IP reaction between PIP and TMC after introducing the *o*-hydroxy porous organic polymer (*o*-POP) (Fig. 7a).[118] Due to electrostatic attraction and hydrogen bonds, *o*-POP raises the viscosity of the solution and slows the diffusion of PIP monomers into the organic phase. As a result of diffusion-driven instability at the IP interface, a polyamide membrane with a crumpled ring-shaped structure was created. The resulting membranes after *o*-POP incorporation displayed higher water permeance (up to 29.9 L m^{-2} h^{-1} bar^{-1}) with high Na_2SO_4 rejection (up to 97.5%).[118] Later, Yuan *et al.* demonstrated the fabrication of an asymmetric polyamide membranes with a highly ordered hollow nanostrip morphology using IP reaction between PIP and TMC.[119] In their research, they used a dendrimer porous layer created by the diazotization-coupling reaction on top of a porous substrate created from polysulfone (PSf) (Fig. 7a). As a result, polyamide membranes with highly uniform nanostrip structures were generated due to the inconsonant amine monomer diffusion rates caused by the dendrimer porous layer. The resulting asymmetric polyamide membrane displays a high water permeance that was up to 3.7–4.3 times higher compared to the conventional polyamide-based TFC membrane while maintaining

high rejection of divalent salt (up to 99.2%).[119] Therefore, the regulation of the diffusivity of the monomers during IP using different organic molecules or polymers in the aqueous or organic solution is a highly efficient technique to control the thickness, surface morphology, and separation performance of the polyamide membranes.

2.2.4 Using additives to control the diffusion of monomers at the aqueous–organic interface. Various salt additives were also employed during interfacial polymerization to tailor the top polyamide selective layer's thickness as the diffusion of monomers at the aqueous–organic interface is influenced by these salt additives. The majority of research studies have focused on the addition of various salts to the aqueous amine monomer solutions in comparison to the organic solution.[13,14] They are effective in demonstrating how their diffusion-controlled IP technique contributes to the development of an ultrathin polyamide selective layer free of defects. In order to control the diffusivity of amine monomers such as PIP, for example, various additives (such as surfactants, phytate molecules, inorganic salts, *etc.*) have been employed.[13,14,37] In order to precisely separate ions and solutes, for example, surfactant molecules were introduced to the aqueous PIP solution to improve the homogeneity of the membrane's sub-nanometer pores.[14] The addition of surfactants speeds up and promotes more uniform amine monomer diffusion during IP at the water–hexane interface. As a result, a polyamide selective layer with uniform pores was created, surpassing those created by conventional interfacial polymerization.[14] Similar to this, stoichiometric equilibrium of the interfacial polymerization reaction was reached after the addition of surfactant molecules (*e.g.*, sodium lauryl sulfate or SLS) in the aqueous PIP solution (Fig. 7a).[13] The developed ultrathin membranes exhibit excellent monovalent to divalent ion selectivity (>1100) and very high Na_2SO_4 rejection of up to 99.95% while maintaining significant water permeance (Table 1).[13] The creation of ultra-permselective polyamide membranes was reported by using electrostatically controlled interfacial polymerization on top of phosphate-rich porous substrates (Fig. 7a).[37] The implication of charged organophosphate (*e.g.*, phytate molecule) coordinated with a ferric ion, helps to enrich the amine monomers by temporarily decelerating its diffusion into the organic phase through electrostatic attraction. As a result, ultrathin polyamide membranes with a thickness of 14 nm were produced that were highly cross-linked and defect-free. The developed ultrathin polyamide membranes show a high water permeance of up to 44.7 L m^{-2} h^{-1} bar^{-1}, a high rejection of Na_2SO_4 of up to 98%, and a low rejection of NaCl of up to 17.5%.[37] Polyamide-based TFC membranes were also created through interfacial polymerization promoted by inorganic salts.[38] The created membranes demonstrated that the addition of salt to the aqueous amine solution regulates the diffusion of amine monomers at the IP interface, modifying the structural nanoscale homogeneity of the polyamide selective layer and thus creating an ultrathin, smooth, and dense membrane. The resulting polyamide membranes exhibit outstanding separation behaviour in terms of both water permeance and salt rejection for FO/RO/NF applications.[38] The creation of an ultrathin, defect-free polyamide selective layer with a high network cross-linking degree is thereby facilitated by salt additives by modulating the diffusion of amine monomers. As a result, employing salt additives during IP considerably enhances the separation efficiency of the resulting ultrathin polyamide-based TFC membranes.

2.2.5 Incorporation of nanostructures to control the diffusion of monomers at the aqueous–organic interface. Despite the use of various organic molecules or polymers and salt additives, different nanostructures were also introduced to regulate the diffusion of monomers. For example, metal–organic frameworks (MOFs),[120] covalent organic frameworks (COF),[36,121] graphene oxide nanosheets,[122] silver nanoparticles,[123] zeolite nanoparticles,[124] MoS_2 nanosheets,[125] TiO_2 nanoparticles,[126,127] carbon quantum dots,[128] MXene particles,[129] MWCNTs,[130] silica nanoparticles,[131] microporous organic nanotubes (MONs),[20] graphitic carbon nitride (g-C_3N_4) nanosheet,[21] nanovehicles,[22] *etc.* were used to fabricate high-performance TFC membranes. More precisely, high-performance polyamide NF membranes were developed using a highly porous and interpenetrated microporous organic nanotube (MONs) layer on top of the PSf porous substrates (Fig. 7a).[20] Based on the molecular simulation study, the MON layer boosts amine storage and reduces amine monomer diffusion into the organic phase, resulting in the development of polyamide membranes with a Turing-type structure with better microporosity, and decreased thickness as low as 15 nm (Table 1 and Fig. 7c). The polyamide membranes regulated by MONs exhibit outstanding separation performance with a high water permeance of up to 41.7 L m^{-2} h^{-1} bar^{-1} and good Cl^-/SO_4^{2-} selectivity for mixed salt solutions (Table 1).[20] In recent studies, graphitic carbon nitride (g-C_3N_4) nanosheets have been introduced into the aqueous PIP solution to create polyamide membranes with organized nanoscale structures as g-C_3N_4 binds with PIP and restricts PIP monomers from diffusing through the IP reaction interface (Fig. 7a).[21] It helps to create a hollow, well-organized structure, enhancing the effective permeable area, and reducing the thickness of the polyamide selective layer. The developed membranes outperform the most advanced NF membranes in terms of exceptional water permeance (up to 105 L m^{-2} h^{-1} bar^{-1}), excellent rejection of Na_2SO_4 (up to 99.4%), and good selectivity between Cl^-/SO_4^{2-} (up to 130).[21] Similar to this, a novel nanoemulsion-regulated interfacial polymerization strategy was also employed to create highly permeable and highly selective polyamide membranes.[22] The nanovehicles, which are oil nanodroplets stabilized by surfactants, assist in concentrating PIP monomers while boosting their diffusion at the IP reaction interface. As a result, a rapid IP reaction takes place, enabling the formation of a highly cross-linked polyamide thin layer. Additionally, it increases the polyamide layer's void fraction and membrane surface area while improving the distribution of pore sizes (Fig. 7d and e). The resulting polyamide membranes exhibit remarkable water permeance (up to 36.8 L m^{-2} h^{-1} bar^{-1}) and excellent Na_2SO_4 rejection (up to 99.6%) (Fig. 7f).[22] Therefore, diffusion-driven IP reaction demonstrates an effective strategy for the creation of ultrathin polyamide membranes. Although, because the reaction is completed in a nanosecond, it is quite difficult to comprehend the exact reaction mechanism. Despite this, the above-discussed technique was

successful in regulating the polyamide layer's thickness, surface area, and degree of cross-linking. These techniques outperformed the performance of the most advanced membrane technology and enhanced the water permeance and separation capabilities of the produced polyamide membranes.

2.2.6 Interlayer-based technique to create ultrathin polyamide membranes. The introduction of nanostructures as an additional layer or as an interlayer between the ultrafiltration (UF) substrate and the top selective layer has gained extensive attention in recent days.[30,32–36,112,132,133] This interlayer helps to maintain the interface flat during the growth of the top selective layer by promoting the storage of amine monomers and their diffusivity towards the organic phase. Many researchers employed these interlayers as an additional layer[30] or as a sacrificial layer[18,19] which was further removed or dissolved following the formation of the top selective layer after interfacial polymerization (Fig. 8a). The top selective layer created on the interlayer-coated porous UF substrate exhibits ultrathin, highly cross-linked, tailored surface textures, and a uniform pore size distribution.[33–35] The TFC membranes made using this method exhibit excellent liquid permeance and high separation performance compared to those made using the conventional fabrication approach.[18] For example, polydopamine-covered single-walled carbon nanotubes (PD/SWCNTs) were used as an interlayer between the polyamide top layer and the PES substrate to fabricate NF membranes. The uniform and smooth structure, high surface porosity, and the hydrophilic nature of PD/SWCNTs interlayer results in the formation of ultrathin (thickness ~12 nm) and defect-free polyamide selective layers (Table 1).[30] The fabricated interlayered-based ultrathin membranes show an excellent water permeance of 32 L m^{-2} h^{-1} bar^{-1} with a moderate rejection rate of Na_2SO_4 (up to 95.9%) (Table 1).[30] In 2015, the nanostrand interlayer was first introduced in order to create freestanding ultrathin nanofilms and their composite membranes for organic solvent nanofiltration (OSN).[18] The sacrificial layer of cadmium hydroxide ($Cd(OH)_2$) nanostrands on top of a porous substrate was deposited through a vacuum filtering approach. The method displays that a defect-free, ultrathin freestanding nanofilm with a thickness of less than 10 nm can be produced owing to the continuous, smooth, hydrophilic, smaller, and uniform pore size of the sacrificial interlayer (Table 1). After the creation of a freestanding ultrathin polyamide nanofilm *via* IP between MPD and TMC, the $Cd(OH)_2$ nanostrand interlayer was removed using hydrochloric acid (Fig. 8a). The crumpled

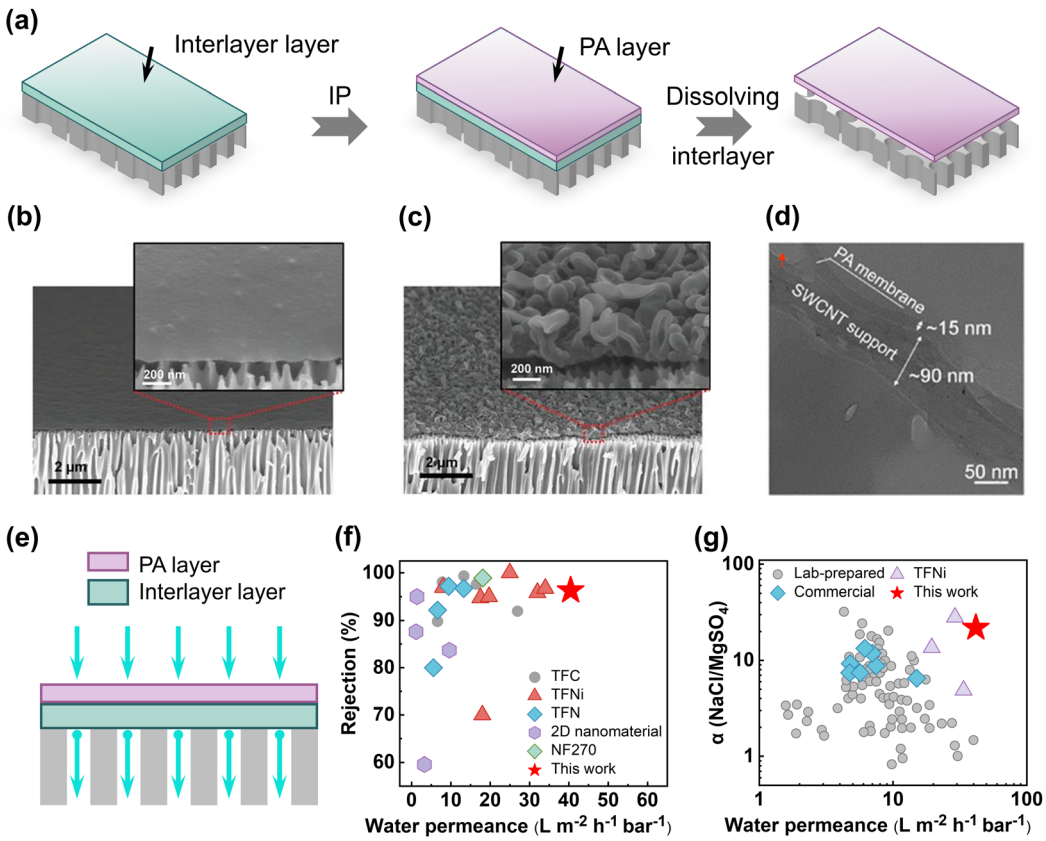

Fig. 8 (a) Illustration of the step-by-step fabrication of ultrathin polyamide nanofilm composite membranes on top of UF substrate membranes using a sacrificial interlayer. (b) and (c) Cross-sectional SEM images of the smooth and crumpled nanofilms formed in the presence of the sacrificial nanostrand interlayer. Reproduced with permission from ref. 18, Copyright 2015, American Association for the Advancement of Science. (d) Cross-sectional TEM image of the ultrathin polyamide membrane prepared on the SWCNT interlayer-coated PES substrates. Reproduced with permission from ref. 34, Copyright 2019, American Chemical Society. (e) Schematic presentation of water transport across interlayered-based TFC membranes. (f) Summary of water permeability and Na_2SO_4 rejection of the state-of-the-art NF membranes reported in the literature. These values are adapted from ref. 34. (g) Water permeability and NaCl/$MgSO_4$ selectivity trade-off of the state-of-the-art NF membranes. These values are adapted from ref. 34.

nanofilms produced on the alumina substrate exhibit outstanding solute separation effectiveness and high acetonitrile permeance (up to 112 L m^{-2} h^{-1} bar^{-1}) (Fig. 8b and c).[18] Later, the synergetic effect of single-walled carbon nanotubes and sacrificial metal–organic framework nanoparticles (*e.g.*, zeolitic imidazolate framework or ZIF-8) was utilized to create a crumpled polyamide TFC NF membrane through interfacial polymerization between PIP and TMC on top of a PES substrate (Fig. 8a).[19] The sacrificial nanoparticle interlayer demonstrates high water permeance (up to 53.5 L m^{-2} h^{-1} bar^{-1}) and an excellent Na_2SO_4 rejection rate (up to 95%) by improving the effective water permeation area.[19] Later in the year 2019, a nanostructure-coated microfiltration substrate (*e.g.*, single-walled carbon nanotubes or SWCNTs) *via* a brush-painting technique was used to fabricate interlayered-based TFC NF membranes (Fig. 8d).[34] The interlayered substrate leads to the successful construction of the ultrathin polyamide top layer, which has a thickness of about 15 nm. The interlayered-based TFC NF membranes show high water permeance (up to 40 L m^{-2} h^{-1} bar^{-1}) and moderate rejection of Na_2SO_4 (up to 96.5%) (Fig. 8e–g).[34] Similar to this, covalent organic framework (COF) nanofibers can also be used as an interlayer on top of the PES substrate to fabricate TFC NF membranes by reacting PIP with TMC.[36] The use of COF nanofibers as an interlayer led to the formation of ultrathin polyamide films (thickness ~20 nm) *via* the controlled release of piperazine monomers to the organic phase (Table 1). The fabricated membranes show a good water permeance of 31.1 L m^{-2} h^{-1} bar^{-1} and a moderate Na_2SO_4 rejection rate (up to 95%) (Table 1).[36] As a result, adding an interlayer or sacrificial layer below the top polyamide selective layer is an efficient approach for creating ultrathin polyamide-based TFC RO/NF membranes with tailored surface morphology and efficient molecular separation performance.

3. Limitations and critical analysis of ultrathin polyamide membranes

Water permeance is significantly impacted by the thickness of the top polyamide selective layer. Undoubtedly, a thinner membrane exhibits exceptional water permeance in comparison to its thicker counterpart. Although polyamide membranes with an ultrathin selective layer demonstrate good separation performance, it is noticed that the rate of increasing water permeance does not follow a linear trend with the reduction of top polyamide layer thickness.[54] The plot illustrating experimental results on how water permeance and permeability varied with various polyamide film thicknesses is presented in Fig. 9a.[54] The observed or apparent water permeance (A_{obs}) was found to increase with decreasing film thickness, but not proportionally. Furthermore, as layer thickness decreases, the observed water permeability (K_{obs}) is reduced. These observations are counterintuitive since for an ideal membrane, the intrinsic water permeability (K_{ideal}) would remain constant regardless of the film thickness, and the water permeance would increase proportionally with decreasing film thickness based on the one-dimensional solution–diffusion model.[134] This phenomenon can be resolved by recognizing that the effective water transport length (l_{eff}) does not directly correlate linearly with the film thickness (l_{PA}) due to the presence of the porous substrate (Fig. 9b and c). As a result, reducing the thickness of the top polyamide selective layer in order to create a highly permeable composite membrane is not as effective as it should be due to the additional hydraulic resistance arising from the substrate geometry in both the normal (or perpendicular to the thickness) and transverse (or diagonal to the thickness) directions. Therefore, for effective water transport, the lateral mass transfer resistance and the normal resistance sitting above the substrate pores are the key factors that hinder the actual water flow while reducing the polyamide film thickness.[55] Therefore, it is necessary to properly understand and overcome these limitations to develop high-performance ultrathin polyamide membranes.

3.1. Role in water transport

3.1.1 Funnel effect and its role in water transport. The transport of water across a conventional TFC membrane involves a complex transport phenomenon known as the funnel effect.[55,135,136] In conventional TFC membranes, water enters

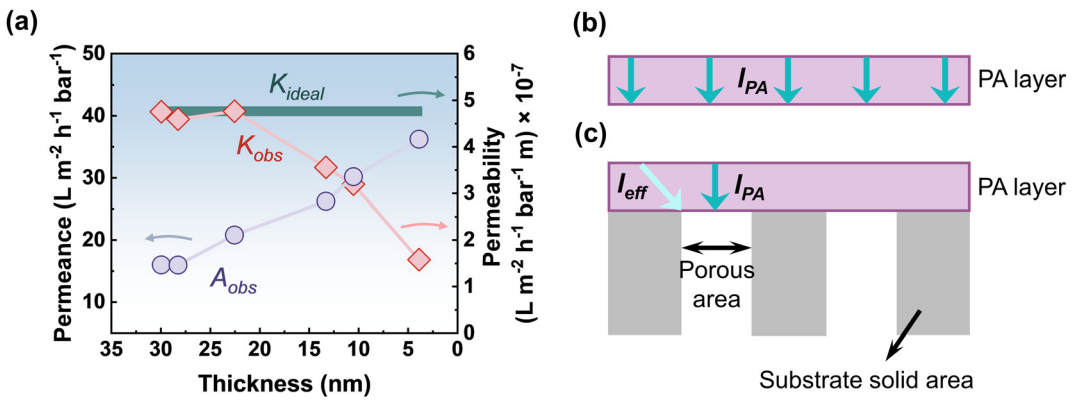

Fig. 9 (a) Plot showing the variation of water permeance and the corresponding permeability of nanofiltration membranes with decreasing thickness of the top polyamide selective layer. These values are adapted from ref. 54, Copyright 2020, American Chemical Society. The illustration shows the transport of water across (b) a freestanding thin film, and (c) a thin film that is supported by a porous substrate membrane. The observed permeability (K_{obs}) decreases as the thickness gets thinner and does not follow the ideal permeability (K_{ideal}) lines as the effective transport length (l_{eff}) is not directly linear with the film thickness (l_{PA}).

far from the pore region and travels along a curved pathway or in the shape of a funnel to exit from the substrate pores (Fig. 10a$_1$).[55] The conventional porous substrates usually have relatively low porosity (equal to or less than 10%) and as a result, water needs to travel both normally and transversely or laterally in order to arrive at the porous zone of the substrate membrane (Fig. 10a$_1$–a$_3$). As a result, the overall transport length of water molecules could be far longer than the rejection layer's thickness ($l_{eff} \gg l_{PA}$), which significantly raises the membrane's hydraulic resistance up to an order of magnitude[135,137,138] and reduces the overall permeance of polyamide composite membranes (Fig. 10b). Modeling studies have also established this phenomenon, showing that for conventional TFC membranes, water is transported along a curved or funnel-shaped path to enter the opening zone of the pores of the substrate membrane.[55,139] As demonstrated by Tang and co-workers[55,140] in Fig. 10c and d, the ideal water permeance of a self-standing/freestanding polyamide film, which remains unaffected by the funnel effect, makes an ideal polyamide-limited upper bound (K_{ideal}/l_{PA}) correlates linearly with the inverse of the film thickness. On the other hand, the substrate-limited lower bound ($\varepsilon K_{ideal}/l_{PA}$) can be obtained by assuming that only the polyamide region above the substrate pore participates in the overall water permeance (Fig. 10c and d). As a result, for typical TFC polyamide membranes where the polyamide selective layer is positioned on top of a porous substrate, the water permeance falls between the upper and lower bound. The study represents that the observed water permeance of the typical TFC membranes on top of the porous substrate is still far from the ideal polyamide-limited upper bound as the porous substrate significantly restricts the transport of water while traveling through the composite structure. The funnel effect is also greatly enhanced for a less uniform flux distribution, which is closely connected to the various transport path lengths while traveling through the composite membrane and leads to a decrease in the effective water permeation rate.[55] Additionally, the inhomogeneity of the water flux distribution is another crucial factor that also facilitates more severe fouling.[137,141] Therefore, the substrate membrane where the selective layer was placed significantly affects the overall water permeance of the polyamide-based TFC membranes.

3.1.2 Role of top layer thickness and substrate porosity on water permeation. The top selective layer's thickness significantly affects the final water permeance of thin film composite membranes. Water molecules need to travel both normally and transversely to arrive at the porous zone of the substrate membrane. As a result, one possible way to increase the water permeance of the composite membranes is by decreasing the transport distance of the water molecules in the normal direction, which can be achieved by reducing the thickness of the top polyamide selective layer (Fig. 10a$_1$ and a$_2$). As demonstrated by Tang and co-workers,[55,140] a thick polyamide selective layer experiences very limited funnel effects on water transport, and as a result the TFC permeance curve remains closer to the lower end of the ideal polyamide-limited upper bound line (Fig. 10c).

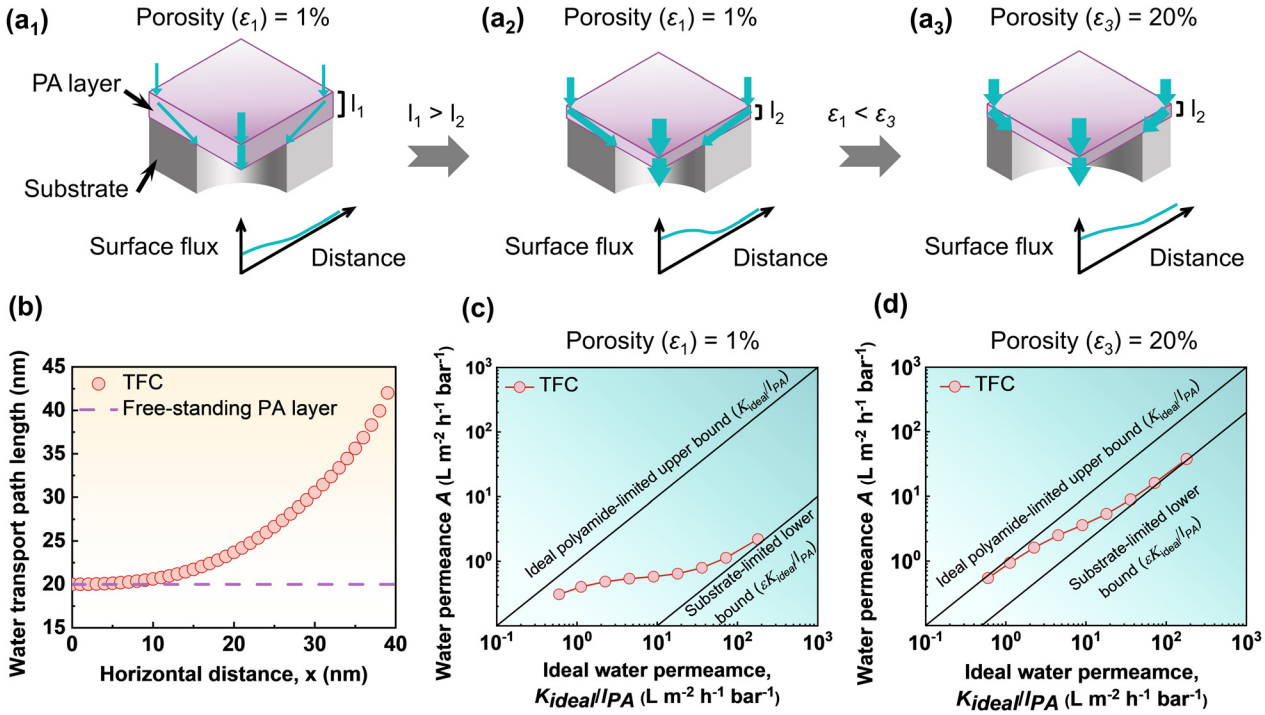

Fig. 10 Schematic view of the transport of water through the polyamide TFC membranes where (a$_1$) and (a$_2$) show the effect of polyamide layer thickness, and (a$_2$) and (a$_3$) show the effect of substrate porosity. (b) The water transport path length in terms of the location of the path of the freestanding polyamide film and the conventional TFC membranes. (c) and (d) The plot shows the relationship between the ideal water permeance for a self-standing/freestanding polyamide film and the available water permeance for TFC membranes with various substrate porosities (ε) at (c) $\varepsilon_1 \sim 1\%$ and (d) $\varepsilon_3 \sim 20\%$. These values are adapted from ref. 55, Copyright 2022, American Chemical Society.

In contrast, for an ultrathin polyamide selective layer, the TFC permeance curve is far away from the ideal polyamide-limited upper bound line; instead, it is approaches asymptotically to the substrate-limited lower bound (Fig. 10c). This implies that when the thickness of the top polyamide selective layer decreases, the substrate generates more geometric restriction, which reduces the actual effectiveness of the ultrathin polyamide TFC membranes (Fig. 10c). Despite this, the creation of ultrathin polyamide membranes is nonetheless a promising strategy to enhance the water permeance of the polyamide TFC membranes.

In addition to the thickness of the top polyamide layer, the performance of polyamide TFC membranes is substantially impacted by the porosity of the substrate membrane. As an example, for low porosity membranes (*e.g.*, porosity, $\varepsilon_1 \sim 1\%$), water molecules need to travel through the membrane substrate's pores in both the normal and transverse directions, requiring longer transport pathways to arrive at the porous zone of the substrate membrane (Fig. 10a$_2$). Whereas for higher porosity membranes (*e.g.*, porosity, $\varepsilon_3 \sim 20\%$), a large number of pores helps to reduce the transverse or lateral distance of the water molecules to arrive at the porous zone of the substrate membrane (Fig. 10a$_3$). In the modeling study by Tang and co-workers,[55,140] it was revealed that the substrate-limited upper bound of the typical TFC membranes approaches the ideal polyamide-limited upper bound when substrate porosity (ε) increases from 1 to 20% by significantly shortening the effective transport distance for water molecules (Fig. 10a$_2$, a$_3$, c and d). As a result, the funnel effect is less pronounced for the higher porosity substrate membrane than for the low porosity substrate membrane. Nevertheless, it is important to note that the fabrication of ultrathin membranes on top of high-porosity substrates could be more challenging, and the resulting membrane may also face poor mechanical stability.

3.1.3 Effective solutions to overcome these limitations

Introduction of an interlayer as a gutter layer. To address the discussed permeation limitations due to the substrate, three layers of composite structures have been developed, with the addition of a third highly permeable interlayer, or the so-called 'gutter' layer between the top polyamide selective layer and the substrate membrane, as illustrated in Fig. 11a$_1$ and a$_2$. In the literature, many researchers introduced numerous high-permeability materials as interlayers or gutter layers. For example, silver nanoparticles,[123,142] 3D porous materials (*e.g.*, metal–organic frameworks,[113] and covalent organic frameworks[36,143]), carbon nanotubes,[32,34,144] 2D materials (*e.g.*, graphene oxide[89,145] and MXene[144,146,147]), tannic acid/Fe^{3+} complexes,[148,149] and polydopamine coatings[150,151] have been extensively employed as an interlayer to enhanced the separation performance of the polyamide-based TFC membranes (Fig. 11a$_1$ and a$_2$). The high permeability interlayer helps to improve the effective water permeance of the TFC membranes by reducing the geometrical restriction that arises from the substrate membrane. The presence of the high permeability interlayer within the polyamide TFC membranes strengthens the water transport channel and results in a more uniform flux distribution.[132] Additionally, the presence of the

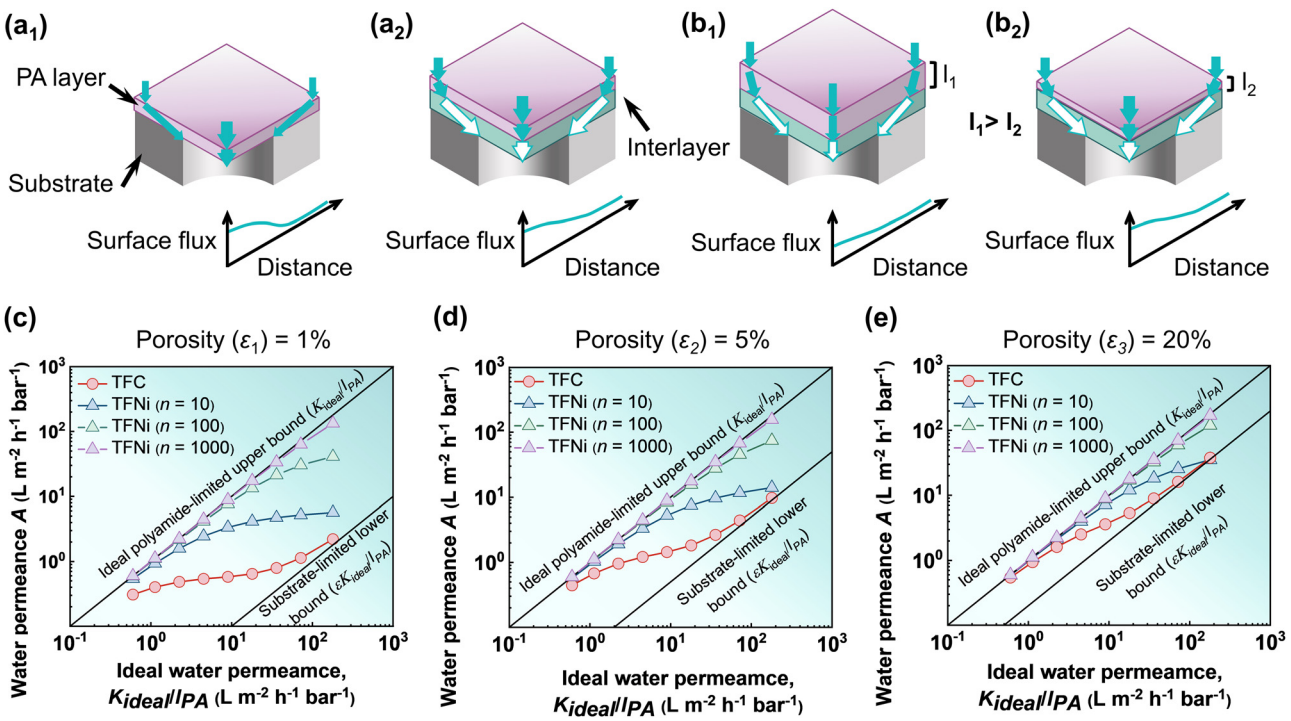

Fig. 11 Schematic view of the water transport through the polyamide TFC membranes where (a$_1$) represents a typical TFC membrane, (a$_2$) represents an interlayered thin-film nanocomposite (TFNi) membrane, and (b$_1$) and (b$_2$) show the effect of polyamide layer thickness. (c)–(e) The plot shows the relationship between the ideal water permeance for a self-standing/freestanding polyamide film and the available water permeance of interlayered TFNi membranes with different relative hydraulic water permeability (for *n* values of 10, 100, and 1000) and with various substrate porosities (ε) at (c) $\varepsilon_1 \sim 1\%$, (d) $\varepsilon_2 \sim 5\%$, and (e) $\varepsilon_3 \sim 20\%$. These values are adapted from ref. 55, Copyright 2022, American Chemical Society.

interlayer may eliminate the extremely high localized flux hotspots, which may in turn reduce the tendency of membrane fouling.[152,153] Besides this, examining the utilization of specific interlayer material chemistry to increase selectivity against targeted contaminants is a promising area for future research.[154–156] Therefore, further research is required to gain a deeper understanding of the gutter layer's impact to further enhance the separation performance of TFC membranes. In order to thoroughly assess the effect of interlayer during the growth of polyamide films, membrane thickness, surface morphology, the degree of cross-linking, and separation performance (*e.g.*, water permeability, selectivity, antifouling properties, chlorine resistance, *etc.*), more modeling and experimental studies need to be conducted. Some 2D analytical models,[157,158] and 3D computational models[139] have previously been utilized to study the impact of the interlayer on water transport through the composite membrane. However, the behavior of membrane transport has not been adequately addressed using this model. An in-depth understanding of the mechanism of water transport through polyamide membranes was critically demonstrated in a recent study by Tang and co-workers[55,140] using a three-dimensional (3D) simulation.[55] The modeling study effectively addressed the influence of the geometry-induced funnel effect and the interlayer-promoted gutter effect in terms of various substrate porosities by plotting the water permeance as a function of ideal water permeance (Fig. 11c–e).[55] Fig. 11c–e reveal that the use of a highly permeable interlayer between the polyamide selective layer and substrate membrane helps to reduce the funnel effect. The addition of the highly permeable interlayer effectively enhances the transport of water molecules in the transverse direction towards the substrate porous area, which minimizes the geometric restriction by reducing the overall hydraulic resistance and the funnel effect. Additionally, relative hydraulic water permeability (n), *i.e.*, the ratio between the water permeability of the interlayer and the top polyamide selective layer, plays a significant role. The influence of relative hydraulic water permeability (n) is also shown in Fig. 11c, which demonstrates that for a high permeable interlayer (as an example, for an n value of 1000), the permeance curve (TFNi for n = 1000) moves closer to the ideal polyamide-limited upper bound. Additionally, in the presence of an interlayer, the substrate porosity also contributes significantly, pushing the permeance curve closer towards the ideal polyamide-limited upper bound (Fig. 11c–e). As seen from Fig. 11c–e, when substrate porosity (ε) increases from 1 to 20%, the permeance curve (TFNi for n = 1000) almost matches with the ideal polyamide-limited upper bound line, resulting in almost 100% water permeance efficiency. As a result, employing a high permeability interlayer with a higher substrate porosity enables the maximum gutter effect and thus completely eliminates the geometrical restrictions imposed by the substrate membrane.

The effect of polyamide selective layer thickness after introducing the interlayer was also investigated through the modeling study (Fig. 11b$_1$, b$_2$, c–e).[55] The modeling analysis reveals that interlayer-based membranes generally exhibit very limited gutter effects on water transport for thicker polyamide selective layers (such as a thickness of 160 or 300 nm) in comparison to the thin polyamide selective layer (Fig. 11c–e). This suggests that, for a very thick polyamide selective layer, the total transport resistance resulting from the substrate membrane is dominated by the transport distance in the normal direction rather than the transverse or lateral direction. As a result, the effectiveness of high permeability interlayers in reducing the transverse transport resistance becomes extremely limited for thicker polyamide TFC membranes. It is therefore more effective to design polyamide membranes with an ultrathin selective layer following the addition of a high permeability interlayer since the gutter effect becomes more prominent in comparison with the thicker polyamide selective layer. Although the creation of ultrathin membranes demonstrates an impressive performance improvement in contrast to the other methods, the funnel effect that arises from the substrate membrane restricts the ideal performance enhancement of the ultrathin membranes. Therefore, the above-discussed mechanism describes how regulating the porosity of the substrate membrane and the introduction of the interlayer could successfully mitigate the existing geometrical restrictions and will considerably help to unleash the potential of ultrathin membranes in future studies.

Creation of crumpled morphology of the polyamide selective layer. According to the literature, a crumpled surface of the top polyamide layer significantly improves the water permeance of the polyamide RO/NF membranes.[116,117,149] The crumpled structure considerably increases the membrane's effective surface area, enabling it to enhance the overall water permeability rate (Fig. 12a$_1$ and a$_2$).[117,140] The improved water permeance of the crumpled membranes has been elucidated through several explanations, including an increased effective surface area for filtration, a thinner polyamide layer, and the promotion of water transport pathways.[140] The performance enhancement in terms of the membrane surface area is summarized and plotted based on literature results (Fig. 12b$_1$). It is interesting to see that the increased membrane surface area alone cannot fully explain the experimentally observed flux enhancement; the experimental data are generally above the theoretical line, suggesting additional mechanisms. This additional mechanism was coined by Tang and co-workers[55,140] introducing the self-gutter effect which greatly shortened the water transport pathways with more uniform flux distribution. As previously discussed, the effective water transport distance (l_{eff}) for a conventional smooth TFC membrane is considerably higher compared to the intrinsic thickness of the top selective layer (l_{PA}), resulting in a significantly elevated funnel effect, lowering the water permeation rate in comparison to the freestanding polyamide film (Fig. 12a$_1$). The funnel effect can be significantly overcome by creating crumple polyamide membranes as they contain free voids on top of the porous substrate, which potentially shorten the effective water transport distance in the polyamide film (Fig. 12a$_2$).[137,139,159] As demonstrated by Tang and co-workers[55,140] the crumpled structure in TFC RO/NF membranes containing nanovoids behaves as a high permeability interlayer, which greatly helps in increasing the water permeation rate by reducing the overall transport pathways. This behavior is similar to the interlayer-

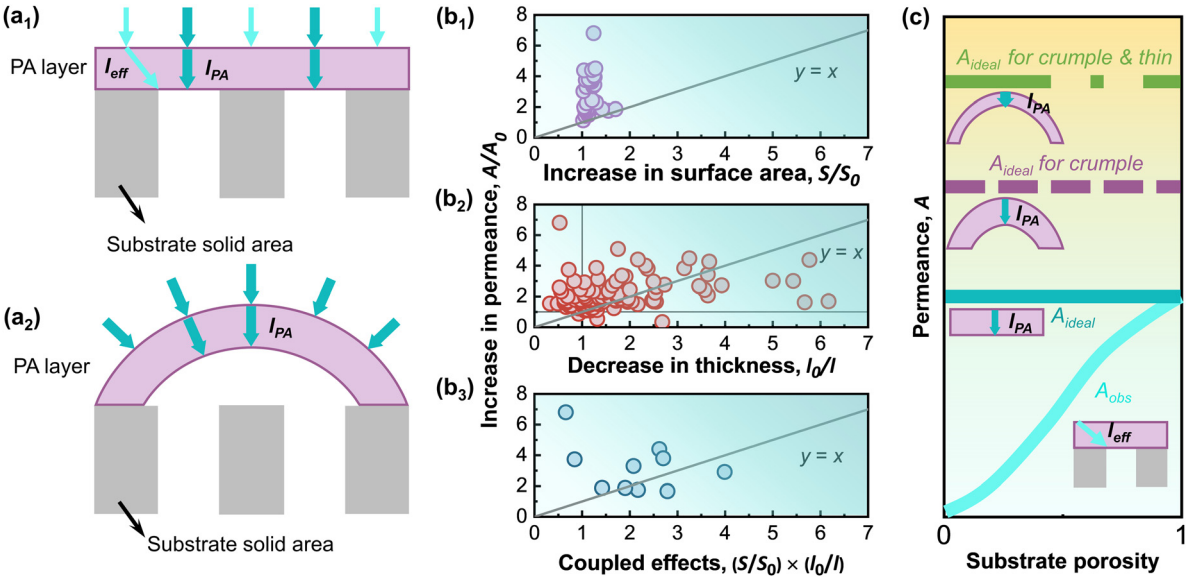

Fig. 12 Schematic view for illustrating the water transport for (a_1) typical TFC membranes, and (a_2) crumpled TFC membranes, where l_{eff} defines the effective transport length, and l_{PA} defines the intrinsic thickness of the top polyamide selective layer. Figures are adapted with permission from ref. 140, Copyright 2022, American Chemical Society. A plot of the literature data on crumpled NF membranes in terms of the increase in permeance with (b_1) an increase in the surface area, (b_2) a decrease in the thickness of the top layer, and (b_3) the couple effects of the surface area combined with the thickness reduction. The theoretical performance improvement resulting from the reduced thickness and surface area is shown by the $y = x$ line. (c) The benchmark of the theoretical water permeance improvement in terms of substrate porosity for a freestanding film, crumple polyamide film, and crumple and thin polyamide film. These values are adapted from ref. 140, Copyright 2022, American Chemical Society.

promoted gutter effect, which is also rationalized as the self-gutter effect, thus contributing to the overall water permeance.[55] The growth of crumpled morphology along with an increase in the membrane surface area is often additionally associated with a decrease in the thickness of the polyamide top selective layer (Fig. 12b_2).[37,160–162] Experimental observations show that the water permeance of crumpled membranes may increase by nearly an order of magnitude, which can be explained by the synergistic effect of reduced polyamide thickness and increased surface area ratio (Fig. 12b_3). As shown in Fig. 12c, the additional advantage of enhanced filtration area causes the water permeance of crumpled membranes to surpass the ideal water permeance of smooth membranes. Whereas, the theoretical results successfully demonstrate that the synergetic action of the crumpled membranes with increasing effective filtration area in combination with the thinner polyamide layer optimizes the water transport channels, leading to the highest enhancement in water permeance (Fig. 12c).[55,140] Therefore, in order to improve the overall membrane separation performance, it appears that the creation of crumpled polyamide films with a thinner or ultrathin rejection layer could provide an excellent approach in future studies and this can be achieved by modulating the monomer's reactivity, which leads to a higher enthalpy of formation, generating more heat and creating strip or crumpled structures.[116,140]

3.2. Role in solute rejection/ion selectivity

Recent progress in TFC RO/NF membrane development has employed a variety of techniques to create highly permeable desalination membranes such as controlling the thickness and effective surface area of the top polyamide selective layer.[18,40,46,117] However, in the creation of ultrathin membranes to increase the water permeability of the polyamide composite membranes, the solute separation or the solute–solute selectivity may be compromised since the structural properties of the top layer have some additional impacts on the overall separation performance. For example, the density and nanoscale structural inhomogeneity of the top polyamide selective layer play a significant role in the membrane transport behavior.[163,164] Therefore, it is highly important to design an ultrathin polyamide membrane with a more homogenous and narrowest density distribution in order to simultaneously enhance water permeance and water–solute or solute–solute selectivity. Additionally, the selectivity of polyamide membranes is substantially influenced by the interior and exterior charge density of the top selective layer.[165] For solute separations through nanofiltration membranes with a thin polyamide selective layer, it is considered that the Donnan exclusion effect (charge–charge repulsion) becomes more significant compared to the steric hindrance exclusion (pore size exclusion).[54] For this reason, the regulation of membrane charge has been widely employed to enhance NF performance.[166–168] Therefore, to design highly selective membranes, a polyamide selective layer with minimum thickness that can generate a significant Donnan exclusion effect and a high degree of network cross-linking is highly desired. Furthermore, since the polyamide-based TFC RO/NF membranes are created on top of a porous substrate to provide mechanical support for the top polyamide selective layer, it is essential to maintain an adequate degree of cross-linking in the network structure when thickness gets reduced. Otherwise, the ultrathin selective layer may collapse

under high pressure and over a long-time operation, which would reduce the effectiveness of the membranes. As a result, the polyamide selective layer needs to maintain a critical thickness range, where it retains the required mechanical strength for sustaining at high operating pressure.[169]

Recommendations for fabricating high-performance ultrathin membranes. The creation of defect-free ultrathin polyamide membranes with highly cross-linked network structures, which are desired for achieving high ionic and molecular selectivity, has been made possible through a number of novel techniques, but producing defect-free membranes across large areas is still quite challenging. For instance, surfactant molecules are frequently employed to create uniform, defect-free sub-nanometer pores in PIP-TMC[13,14] and MPD-TMC[170,171] based membranes for precise ion and solute separation. In addition, by creating the top polyamide selective layer with an asymmetrical structure, it is possible to significantly enhance the selective separation of ions or solutes. Due to the self-limiting nature of the interfacial polymerization reaction, the typical polyamide layer usually has an asymmetric structure, with a loosely packed segment at the top of the film facing the organic acyl chloride phase and a highly packed segment underneath the film facing the aqueous amine phase (Fig. 13a).[13,172] In this asymmetric polyamide structure, the top loose layer is responsible for high permeability, while the lower dense layer is responsible for high ion selectivity during the filtration process. However, this type of asymmetric polyamide structure is prone to more severe concentration polarization and higher fouling, thus significantly lowering the overall separation efficiency of the composite membranes (Fig. 13a). Therefore, a novel type of asymmetric polyamide structure is required to overcome these drawbacks. Earlier, an asymmetrical ultrathin polyamide selective layer was designed by utilizing the dual interfacial polymerization strategy which consists of a top dense layer and a loose polypiperazinamide sublayer, where the relatively looser layer acts as an interlayer, resulting in an improvement in permeability of up to 2.5 times while maintaining high salt rejections.[173] However, the creation of an asymmetric polyamide layer using the dual IP strategy requires a complex fabrication process. To overcome this limitation, it may be possible to create an ultrathin polyamide membrane with an asymmetric structure by varying the monomer concentration from low to high by using the well-established electrospray method in a more straightforward and adaptable way (Fig. 13b).[45,47,90] This method will help in forming a novel asymmetric polyamide structure (Fig. 13b) where the higher permeability loose polyamide layer acts as an interlayer-promoted gutter effect (or self-gutter effect) and reduce the overall transport pathways, thus significantly increasing the water permeation rate while maintaining high solute selectivity (Fig. 13b). At the same time, engineering the polyamide structure in this way will result in asymmetric charge distribution, and possibly a charge reversal effect will be observed. This effect may improve the separation ability of cations (*e.g.*, Mg^{2+} and Ca^{2+}) over anions (*e.g.*, SO_4^{2-}) of the conventional PIP-TMC-based polyamide membranes, which may be helpful for water softening. Additionally, the top dense layer may encounter less concentration polarization and less fouling, which would greatly contribute to the membrane's overall separation performance (Fig. 13b). Despite these strategies, further techniques are still required to create high-performance ultrathin polyamide membranes.

4. Implications and future perspectives

4.1. Implications of ultrathin membranes in real-field applications

Ultrathin membranes offer numerous advantages in real-field applications, with the potential to revolutionize industries such as water, chemical, and pharmaceutical sectors. These membranes feature high efficiency, low energy consumption,[23] and low maintenance requirements, making them an ideal choice for many industries. Despite the potential advantages, the fabrication of ultrathin membranes for real-field applications may face challenges on the industrial scale. In particular,

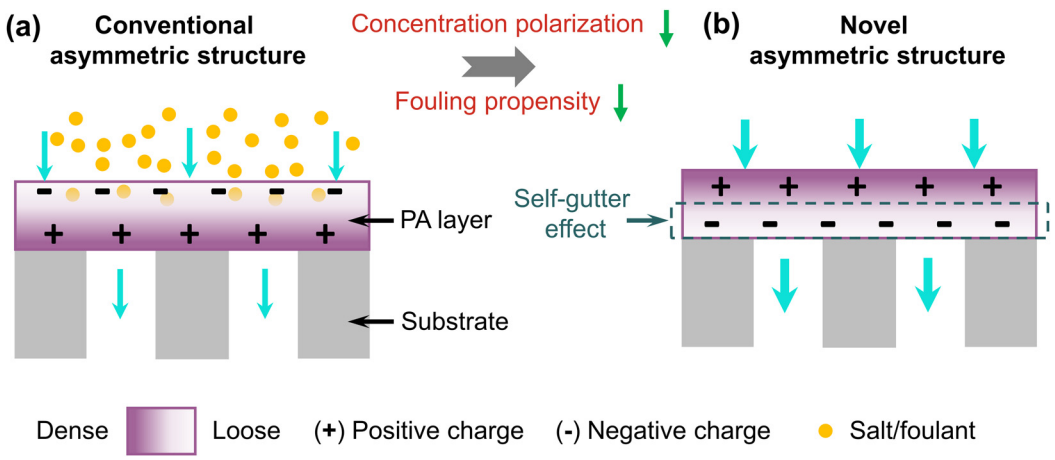

Fig. 13 Schematic view of asymmetric polyamide membranes on top of a porous substrate where (a) shows the conventional asymmetric polyamide structure, and (b) shows the novel asymmetric polyamide structure.

achieving the required rejection/selectivity may need a structure that is highly cross-linked and free from defects. In this regard, approaches such as electrospray,[45,48,174] which intrinsically tend to produce a large number of defects, generally show lower rejections (Table 1) and are thus less preferred. In the future development of ultrathin membranes, it is crucial to emphasize on defect control and structural integrity for large-scale membrane productions. The development of novel emerging membrane materials and new fabrication techniques may further enhance their feasibility, fulfilling their application demands as potential alternatives to conventional membranes.

4.2. Implications to other emerging membrane materials and their commercial scale viability

Even though many approaches are outlined for creating high-performance ultrathin polyamide-based TFC membranes, some of the strategies highlighted in Section 3.1.3 can be potentially relevant for other newly developed emerging materials to boost their separation performance by successfully decreasing the water transport path, lowering the hydraulic resistance and minimizing the funnel effect. For example, aquaporin-based biomimetic membranes (AQPs),[175–177] aligned carbon nanotube (CNT)-based membranes,[178,179] synthetically designed nanochannels,[180–182] nanoporous graphene membranes (NPG),[183,184] MOF/COF membranes,[185,186] and 2D graphene-based membranes,[187] all experience the aforementioned geometric restriction due to the substrate membrane. Therefore, minimizing the transport pathways by creating ultrathin membranes with crumpled morphology or introducing interlayers with different surface chemistry between these newly developed membranes and the substrate membranes can be a beneficial and adaptable way for customizing the performance of emerging membrane materials (Fig. 14).

For industrial applications, large-scale roll-to-roll production of the newly designed ultrathin membranes and emerging membrane materials is of utmost importance. In Fig. 14, we have qualitatively plotted the performance and commercial scale feasibility comparison of the traditional membranes, the ultrathin membrane with a crumpled structure, the ultrathin membrane with an interlayer and several novel membrane materials.[188–190] The vertical axis shows the (possible) membrane performance improvement with respect to water permeance, while the horizontal axis indicates the commercial viability based on scalable technology and fabrication expenses. Although newly developed membrane materials offer great separation performance, they often face challenges when it comes to large scale roll-to-roll manufacturing. As an example, graphene-based membranes may be produced at large scales, whereas other emerging membrane materials like AQPs,[9] CNTs,[9] nanoporous graphene (NPG),[191] 2D graphene-based[187] membranes, and MOF[185] membranes, pose challenges for commercial scale-up and thus demand highly specialized manufacturing techniques. Additionally, further research will be required in order to fully exploit the potential applications and technological viability of these membranes.

4.3. Utilization of ultrathin membranes in other applications

Organic solvent nanofiltration (OSN). Organic solvent nanofiltration (OSN) serves as a promising energy-efficient membrane-based technology for ionic and molecular separation in harsh organic solvents.[192,193] OSN has been widely employed in the pharmaceutical purification processes as well

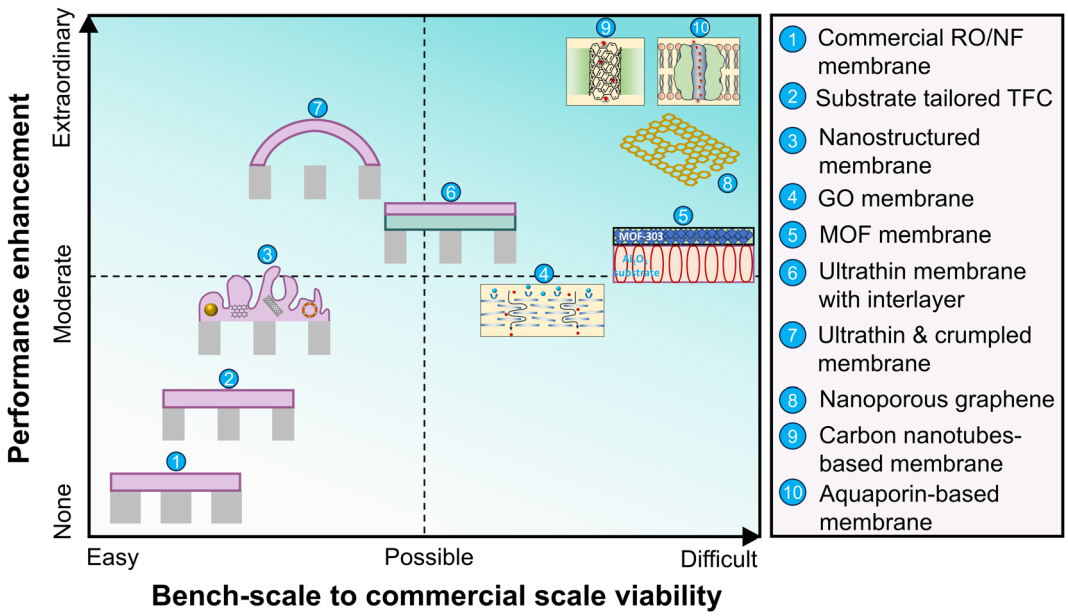

Fig. 14 The plot demonstrates the comparison of the traditional TFC membrane, the ultrathin membrane with a crumpled structure, the ultrathin membrane with an interlayer, and newly emerging membrane materials in terms of their performance and commercial scale viability. The figure adopted with an upgraded evaluation framework similar to the one published by Pendergast *et al.* (ref. 188), Yang *et al.* (ref. 189), and Guo *et al.* (ref. 190).

as solvent recovery, organic synthesis, and the refining industry.[193] In recent years, solute/solvent recovery and solvent exchange remain the two main applications that involve the membrane-based separation technology. The major objective of current research is the utilization of OSN membranes to further expand the upper bound of the permeability and selectivity trade-off. This was accomplished by utilizing a variety of novel membrane materials and cutting-edge fabrication methods that exhibit high solvent permeance, high selectivity, and long-term stability in organic solvents.[18,194–196] However, next-generation OSN membranes are still required with high permeance for both polar and non-polar solvents while maintaining high solvent permeance and selectivity. Therefore, the process of employing ultrathin membranes with novel fabrication protocols (*e.g.*, creation of crumpled morphology or introduction of an interlayer) could be beneficial for future research and further improving the performance of OSN membranes (Fig. 15).

Membrane-based gas separation. To meet the needs of industrial gas separations (such as hydrogen recovery, carbon capture, natural gas purification, hydrocarbon separation, *etc.*), TFC membranes are currently attracting more interest.[197] For instance, ultrathin microporous nanofilm-based membranes can be utilized for gas and hydrocarbon separations in the petrochemical industry.[196] However, the main challenges in the creation of high-specification TFC membranes for gas separation applications still remain unexplained, which include the thickness-dependent gas permeability and the geometrical restriction that arises from the substrate membrane.[139] Despite this, permeability and selectivity also have a trade-off relationship that affects how effective a membrane is for gas separation applications. As a result, the main goal of current research in membrane-based gas separation technology is to extend the upper bound line of the permeability and selectivity trade-off. It is beneficial to address energy and environmental issues using a gas separation membrane technique that is both energy-efficient and eco-friendly. In view of this, the fabrication protocols implemented for ultrathin polyamide-based TFC membranes by optimizing the transport path of gas molecules may have the potential to achieve the desired performance of gas separation applications in the near future (Fig. 15).

Other potential applications. Membrane-based technology has been extensively utilized in a number of other recent applications. For example, TFC-based pervaporation membranes have been developed for the separation of liquid–liquid mixtures.[198] Additionally, membrane contactors (MC) have been employed for removing a variety of contaminants from wastewater including volatile organic compounds (VOCs), phenols, toluene, heavy metals, ammonia, *etc.*[199] Furthermore, TFC-based NF membranes also perform well in the field of salt–lithium separation, since they are cheaper and require less energy than traditional lithium extraction methods (such as solvent extraction, adsorption, precipitation, ion exchange, *etc.*).[200] Future development of high-performance TFC membranes for this type of application still faces difficulties and therefore, it is necessary to enhance the performance of TFC membranes, which may be achieved by employing ultrathin membranes along with the newly designed fabrication methods (Fig. 15). In addition to the effectiveness of ultrathin membranes achieved through novel fabrication strategies, new or modified manufacturing methods must be designed to overcome the difficulties encountered during the transition from laboratory scale to module-scale production (Fig. 15).[201]

5. Conclusions

The most recent research on ultrathin polyamide-based membranes, limitations, and potential solutions with future perspectives have been outlined here. As the top selective layer is crucial for the transportation of water or solvents, it is a promising approach for reducing the top selective layer's thickness in order to enhance the overall membrane performance. In this review, we provide a thorough investigation into the creation of ultrathin membranes by optimizing the interfacial polymerization process and employing a variety of novel fabrication methods. We critically assessed the drawbacks associated with ultrathin membranes resulting from the substrate membrane, and discussed, some potential strategies to enhance the performance of ultrathin polyamide membranes. We also explained how these strategies will improve the performance of the ultrathin membranes when utilized for both existing and newly developed membrane materials. A qualitative

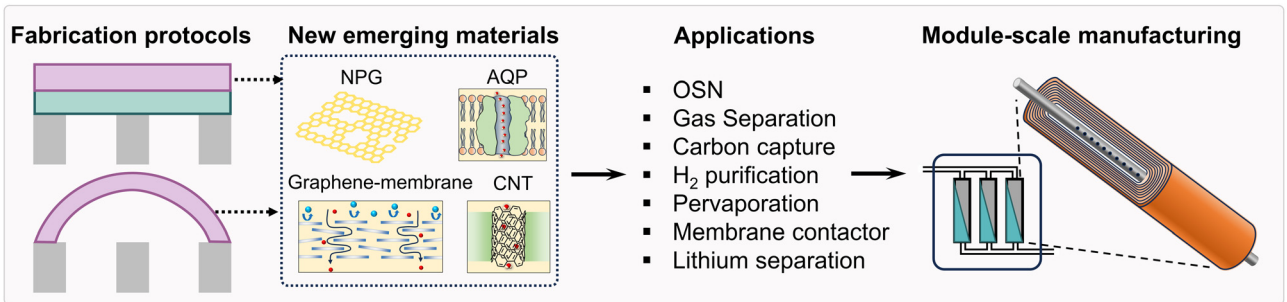

Fig. 15 Schematic presentation of the future perspectives and remaining challenges to fully unleash the effectiveness of new emerging membrane materials using novel fabrication protocols. The figure of the membrane module is adapted with permission from ref. 201, Copyright 2023, American Association for the Advancement of Science.

assessment of the performance and commercial scale feasibility of various traditional membranes and novel membrane materials is also presented. Overall, the primary focus for future research needs to be the scaling up of membrane production and the production of membrane modules for industrial purposes.

Abbreviations

A	Water permeance
AFM	Atomic force microscopy
A_{obs}	Observed or apparent water permeance
AQPs	Aquaporins
CNTs	Carbon nanotubes
COF	Covalent organic frameworks
CVD	Chemical vapor deposition
DLC	Diamond-like carbon
DMF	Dimethylformamide
DSC	Dual-layer slot coating
FO	Forward osmosis
GO	Graphene oxide
g-C_3N_4	Graphitic carbon nitride
IP	Interfacial polymerization
K_{ideal}	$P^{H}_{w,PA}$ or ideal/intrinsic water permeability of the polyamide layer
K_{ideal}/l_{PA}	Ideal water permeance of the freestanding film
LbL	Layer-by-layer
l_{eff}	Effective water transport length
l_{PA}	Thickness of the polyamide layer
MF	Microfiltration
mLbL	Molecular layer-by-layer
MOF	Metal–organic framework
MONs	Microporous organic nanotube
MPD	*m*-Phenylenediamine
n	Relative hydraulic water permeability
NF	Nanofiltration
NPG	Nanoporous graphene
OSN	Organic solvent nanofiltration
PA	Polyamide
PAA	Polyacrylic acid
PAN	Polyacrylonitrile
PCS	Phytate-coordinated substrate
PD/PDA	Polydopamine
PEI	Polyethylene imine
PES	Polyether sulfone
PIP	Piperazine
PSf	Polysulfone
PVA	Polyvinyl alcohol
RO	Reverse osmosis
SEM	Scanning electron microscope
SLS	Sodium lauryl sulfate
SWCNT	Single-walled carbon nanotubes
TAPB	1,3,5-Tris(4-aminophenyl)benzene
TAPM	Tetrakis(4-aminophenyl)methane
TEM	Transmission electron microscope
TFC	Thin-film composite
TFNi	Interlayered thin-film nanocomposite
TMC	Trimesoyl chloride
TPMC	Tetraphenyl-methane-4,4′,4″,4‴-tetraacyl chloride
UF	Ultrafiltration
ZIF-8	Zeolitic imidazolate framework
ε	Substrate porosity

Conflicts of interest

There are no conflicts to declare.

Acknowledgements

This study was supported by the General Research Fund (project no: 17201921 and 17206122) of the Research Grants Council of Hong Kong. This work was also partially supported by the Innovation and Technology Fund (project no: GHP/181/20GD) of the Hong Kong Special Administrative Region, China, and the RGC Senior Research Fellow Scheme from the Research Grants Council of the Hong Kong Special Administration Region, China (project no: SRFS2021-7S04). Publication was made possible in part by support from the HKU Libraries Open Access Author Fund sponsored by the HKU Libraries.

References

1 R. I. McDonald, P. Green, D. Balk, B. M. Fekete, C. Revenga, M. Todd and M. Montgomery, *Proc. Natl. Acad. Sci. U. S. A.*, 2011, **108**, 6312–6317.
2 P. H. Gleick, *Proc. Natl. Acad. Sci. U. S. A.*, 2018, **115**, 8863–8871.
3 M. Elimelech, *J. Water Supply: Res. Technol. – AQUA*, 2006, **55**, 3–10.
4 M. A. Shannon, P. W. Bohn, M. Elimelech, J. G. Georgiadis, B. J. Mariñas and A. M. Mayes, *Nature*, 2008, **452**, 301–310.
5 E. Curcio and E. Drioli, *Sep. Purif. Rev.*, 2005, **34**, 35–86.
6 X. Zhou, F. Zhao, P. Zhang and G. Yu, *ACS Mater. Lett.*, 2021, **3**, 1112–1129.
7 C. Y. Tang, Z. Yang, H. Guo, J. J. Wen, L. D. Nghiem and E. Cornelissen, *Environ. Sci. Technol.*, 2018, **52**, 10215–10223.
8 M. Elimelech and W. A. Phillip, *Science*, 2011, **333**, 712–717.
9 J. R. Werber, C. O. Osuji and M. Elimelech, *Nat. Rev. Mater.*, 2016, **1**, 1–15.
10 K. Wang, X. Wang, B. Januszewski, Y. Liu, D. Li, R. Fu, M. Elimelech and X. Huang, *Chem. Soc. Rev.*, 2022, **51**, 672–719.
11 X. Lu and M. Elimelech, *Chem. Soc. Rev.*, 2021, **50**, 6290–6307.
12 R. Zhang, Y. Liu, M. He, Y. Su, X. Zhao, M. Elimelech and Z. Jiang, *Chem. Soc. Rev.*, 2016, **45**, 5888–5924.
13 P. Sarkar, S. Modak and S. Karan, *Adv. Funct. Mater.*, 2021, **31**, 2007054.

14 Y. Liang, Y. Zhu, C. Liu, K.-R. Lee, W.-S. Hung, Z. Wang, Y. Li, M. Elimelech, J. Jin and S. Lin, *Nat. Commun.*, 2020, **11**, 2015.
15 P. Sarkar, S. Modak, S. Ray, V. Adupa, K. A. Reddy and S. Karan, *J. Mater. Chem. A*, 2021, **9**, 20714–20724.
16 H. Peng, W. H. Zhang, W. S. Hung, N. Wang, J. Sun, K. R. Lee, Q. F. An, C. M. Liu and Q. Zhao, *Adv. Mater.*, 2020, **32**, 2001383.
17 B.-Q. Huang, Y.-J. Tang, Z.-X. Zeng, S.-M. Xue, C.-H. Ji and Z.-L. Xu, *ACS Appl. Mater. Interfaces*, 2020, **12**, 35523–35531.
18 S. Karan, Z. Jiang and A. G. Livingston, *Science*, 2015, **348**, 1347–1351.
19 Z. Wang, Z. Wang, S. Lin, H. Jin, S. Gao, Y. Zhu and J. Jin, *Nat. Commun.*, 2018, **9**, 2004.
20 S. Han, J. Zhu, A. A. Uliana, D. Li, Y. Zhang, L. Zhang, Y. Wang, T. He and M. Elimelech, *Nat. Commun.*, 2022, **13**, 7954.
21 C. Zhao, Y. Zhang, Y. Jia, B. Li, W. Tang, C. Shang, R. Mo, P. Li, S. Liu and S. Zhang, *Nat. Commun.*, 2023, **14**, 1112.
22 R. Dai, H. Zhou, T. Wang, Z. Qiu, L. Long, S. Lin, C. Y. Tang and Z. Wang, *Nat. Water*, 2023, **1**, 281–290.
23 Z. Yang, C. Wu and C. Y. Tang, *Water Res. X*, 2023, **19**, 100172.
24 D. Cohen-Tanugi, R. K. McGovern, S. H. Dave, J. H. Lienhard and J. C. Grossman, *Energy Environ. Sci.*, 2014, **7**, 1134–1141.
25 J. Tian, H. Chang, S. Gao, Y. Zong, B. Van der Bruggen and R. Zhang, *J. Membr. Sci.*, 2021, **634**, 119450.
26 Z. Jiang, S. Karan and A. G. Livingston, *Adv. Mater.*, 2018, **30**, 1705973.
27 S.-J. Park, W. Choi, S.-E. Nam, S. Hong, J. S. Lee and J.-H. Lee, *J. Membr. Sci.*, 2017, **526**, 52–59.
28 L. Paseta, C. Echaide-Górriz, C. Téllez and J. Coronas, *Green Chem.*, 2021, **23**, 2449–2456.
29 W. Li, Z. Yang, W. Yang, H. Guo and C. Y. Tang, *AIChE J.*, 2022, **68**, e17517.
30 Y. Zhu, W. Xie, S. Gao, F. Zhang, W. Zhang, Z. Liu and J. Jin, *Small*, 2016, **12**, 5034–5041.
31 S. Xue, C.-W. Lin, C. Ji, Y. Guo, L. Liu, Z. Yang, S. Zhao, X. Cai, Q. J. Niu and R. B. Kaner, *Nano Lett.*, 2022, **22**, 1039–1046.
32 Z. Zhou, Y. Hu, C. Boo, Z. Liu, J. Li, L. Deng and X. An, *Environ. Sci. Technol. Lett.*, 2018, **5**, 243–248.
33 R. Dai, J. Li and Z. Wang, *Adv. Colloid Interface Sci.*, 2020, **282**, 102204.
34 S. Gao, Y. Zhu, Y. Gong, Z. Wang, W. Fang and J. Jin, *ACS Nano*, 2019, **13**, 5278–5290.
35 G. Gong, P. Wang, Z. Zhou and Y. Hu, *ACS Appl. Mater. Interfaces*, 2019, **11**, 7349–7356.
36 Z. Zhang, X. Shi, R. Wang, A. Xiao and Y. Wang, *Chem. Sci.*, 2019, **10**, 9077–9083.
37 X. You, K. Xiao, H. Wu, Y. Li, R. Li, J. Yuan, R. Zhang, Z. Zhang, X. Liang, J. Shen and Z. Jiang, *Iscience*, 2021, **24**, 102369.
38 L. Shen, R. Cheng, M. Yi, W.-S. Hung, S. Japip, L. Tian, X. Zhang, S. Jiang, S. Li and Y. Wang, *Nat. Commun.*, 2022, **13**, 500.
39 H. Qian, S. Li, J. Zheng and S. Zhang, *Langmuir*, 2012, **28**, 17803–17810.
40 J. E. Gu, S. Lee, C. M. Stafford, J. S. Lee, W. Choi, B. Y. Kim, K. Y. Baek, E. P. Chan, J. Y. Chung and J. Bang, *Adv. Mater.*, 2013, **25**, 4778–4782.
41 W. Choi, J.-E. Gu, S.-H. Park, S. Kim, J. Bang, K.-Y. Baek, B. Park, J. S. Lee, E. P. Chan and J.-H. Lee, *ACS Nano*, 2015, **9**, 345–355.
42 X. Shui, J. Li, M. Zhang, C. Fang and L. Zhu, *J. Membr. Sci.*, 2021, **628**, 119249.
43 Z. Zhou, S. Zhou, X. Cheng, W. Liu, R. Wu, J. Wang, B. Liu, J. Zhu, B. Van der Bruggen and Y. Zhang, *Sep. Purif. Technol.*, 2022, **288**, 120648.
44 Y. Liu, H. Wu, H. Zhang, J. Wang and Z. Wang, *Vacuum*, 2023, **207**, 111645.
45 X.-H. Ma, Z. Yang, Z.-K. Yao, H. Guo, Z.-L. Xu and C. Y. Tang, *Environ. Sci. Technol. Lett.*, 2018, **5**, 117–122.
46 M. R. Chowdhury, J. Steffes, B. D. Huey and J. R. McCutcheon, *Science*, 2018, **361**, 682–686.
47 S. Yang, J. Wang, L. Fang, H. Lin, F. Liu and C. Y. Tang, *J. Membr. Sci.*, 2020, **602**, 117971.
48 J. Chen, J. Zhang, X. Wu, X. Cui, W. Li, H. Zhang, J. Wang, X.-Z. Cao and P. Zhang, *J. Mater. Chem. A*, 2020, **8**, 9160–9167.
49 S.-J. Park, W.-G. Ahn, W. Choi, S.-H. Park, J. S. Lee, H. W. Jung and J.-H. Lee, *J. Mater. Chem. A*, 2017, **5**, 6648–6655.
50 S.-J. Park and J.-H. Lee, *J. Membr. Sci.*, 2020, **614**, 118449.
51 S. Badalov and C. J. Arnusch, *J. Membr. Sci.*, 2016, **515**, 79–85.
52 C. Wang, M. J. Park, R. R. Gonzales, S. Phuntsho, H. Matsuyama, E. Drioli and H. K. Shon, *J. Membr. Sci.*, 2022, **655**, 120582.
53 M. J. Park, C. Wang, R. R. Gonzales, S. Phuntsho, H. Matsuyama, E. Drioli and H. K. Shon, *Desalination*, 2022, **541**, 116027.
54 C. Jiang, L. Zhang, P. Li, H. Sun, Y. Hou and Q. J. Niu, *ACS Appl. Mater. Interfaces*, 2020, **12**, 25304–25315.
55 F. Wang, Z. Yang and C. Y. Tang, *ACS EST Engg.*, 2022, **2**, 2023–2033.
56 S. Gao, D. Wang, W. Fang and J. Jin, *Adv. Mater. Technol.*, 2020, **5**, 1901069.
57 S. Zhang, L. Shen, H. Deng, Q. Liu, X. You, J. Yuan, Z. Jiang and S. Zhang, *Adv. Mater.*, 2022, **34**, 2108457.
58 P. W. Morgan, *Condensation polymers: by interfacial and solution methods*, Interscience Publishers, New York, 1965.
59 E. L. Wittbecker and P. W. Morgan, *J. Polym. Sci.*, 1959, **40**, 289–297.
60 P. W. Morgan and S. L. Kwolek, *J. Polym. Sci.*, 1959, **40**, 299–327.
61 S. Zhou, L. Long, Z. Yang, S. L. So, B. Gan, H. Guo, S.-P. Feng and C. Y. Tang, *Environ. Sci. Technol.*, 2022, **56**, 10279–10288.
62 L. Lin, C. Feng, R. Lopez and O. Coronell, *J. Membr. Sci.*, 2016, **498**, 167–179.
63 D. Poncelet, B. P. De Smet and R. J. Neufeld, *J. Membr. Sci.*, 1990, **50**, 249–267.
64 G.-Y. Chai and W. B. Krantz, *J. Membr. Sci.*, 1994, **93**, 175–192.

65 L. Danicher, P. Gramain, Y. Frère and A. Le Calvé, *React. Funct. Polym.*, 1999, **42**, 111–125.
66 A. N. Storey, W. Zhang, J. F. Douglas and F. W. Starr, *Macromolecules*, 2020, **53**, 9654–9664.
67 K. Takamura, M. Koishi and T. Kondo, *J. Pharm. Sci.*, 1973, **62**, 610–612.
68 K. Tiwari, S. Modak, P. Sarkar, S. Ray, V. Adupa, K. A. Reddy, S. K. Pramanik, A. Das and S. Karan, *iScience*, 2022, **25**, 104027.
69 P. Sarkar, T. Sarkar, H. Singh, B. Sutariya, S. Ray, A. Das, S. K. Pramanik and S. Karan, *J. Mater. Chem. A*, 2023, **11**, 14390–14403.
70 F. MacRitchie, *Trans. Faraday Soc.*, 1969, **65**, 2503–2507.
71 P. Zhang, F. Zhang, C. Zhao, S. Wang, M. Liu and L. Jiang, *Angew. Chem.*, 2016, **128**, 3679–3683.
72 J. Ji, J. M. Dickson, R. F. Childs and B. E. Mccarry, *Macromolecules*, 2000, **33**, 624–633.
73 L. Janssen and K. Te Nijenhuis, *J. Membr. Sci.*, 1992, **65**, 59–68.
74 Y. Zhang, N. E. Benes and R. G. H. Lammertink, *Lab Chip*, 2015, **15**, 575–580.
75 R. Arshady, *J. Microencapsulation*, 1989, **6**, 13–28.
76 J. J. Richardson, M. Björnmalm and F. Caruso, *Science*, 2015, **348**, aaa2491.
77 X. Song, S. Qi, C. Y. Tang and C. Gao, *J. Membr. Sci.*, 2017, **540**, 10–18.
78 J. J. Richardson, J. Cui, M. Bjornmalm, J. A. Braunger, H. Ejima and F. Caruso, *Chem. Rev.*, 2016, **116**, 14828–14867.
79 Y. Li, X. Wang and J. Sun, *Chem. Soc. Rev.*, 2012, **41**, 5998–6009.
80 A. Qi, P. Chan, J. Ho, A. Rajapaksa, J. Friend and L. Yeo, *ACS Nano*, 2011, **5**, 9583–9591.
81 G. Decher, *Science*, 1997, **277**, 1232–1237.
82 S. U. Hong, R. Malaisamy and M. L. Bruening, *J. Membr. Sci.*, 2006, **283**, 366–372.
83 A. El-Hashani, A. Toutianoush and B. Tieke, *J. Membr. Sci.*, 2008, **318**, 65–70.
84 C. Wang, M. J. Park, H. Yu, H. Matsuyama, E. Drioli and H. K. Shon, *J. Membr. Sci.*, 2022, 120926.
85 V. Chernikova, O. Shekhah and M. Eddaoudi, *ACS Appl. Mater. Interfaces*, 2016, **8**, 20459–20464.
86 R. Weitz, L. Harnau, S. Rauschenbach, M. Burghard and K. Kern, *Nano Lett.*, 2008, **8**, 1187–1191.
87 Y. Zhang, C. A. D'Ambra, R. Katsumata, R. L. Burns, M. H. Somervell, R. A. Segalman, C. J. Hawker and C. M. Bates, *ACS Appl. Mater. Interfaces*, 2019, **11**, 21177–21183.
88 P. A. Chiarelli, M. S. Johal, J. L. Casson, J. B. Roberts, J. M. Robinson and H. L. Wang, *Adv. Mater.*, 2001, **13**, 1167–1171.
89 X. Kang, X. Liu, J. Liu, Y. Wen, J. Qi and X. Li, *Appl. Surf. Sci.*, 2020, **508**, 145198.
90 A. Jaworek and A. T. Sobczyk, *J. Electrostat.*, 2008, **66**, 197–219.
91 R. Bernstein, C. E. Singer, S. P. Singh, C. Mao and C. J. Arnusch, *J. Membr. Sci.*, 2018, **548**, 73–80.
92 S. Badalov, Y. Oren and C. J. Arnusch, *J. Membr. Sci.*, 2015, **493**, 508–514.
93 M. Fathizadeh, H. N. Tien, K. Khivantsev, J.-T. Chen and M. Yu, *J. Mater. Chem. A*, 2017, **5**, 20860–20866.
94 H. S. Ji, W.-G. Ahn, I. Kwon, J. Nam and H. W. Jung, *Chem. Eng. Sci.*, 2016, **143**, 122–129.
95 S. D. Taylor and A. N. Hrymak, *Chem. Eng. Sci.*, 1999, **54**, 909–918.
96 J. Nam and M. S. Carvalho, *J. Fluid Mech.*, 2009, **631**, 397–417.
97 N. A. Khan, R. Zhang, H. Wu, J. Shen, J. Yuan, C. Fan, L. Cao, M. A. Olson and Z. Jiang, *J. Am. Chem. Soc.*, 2020, **142**, 13450–13458.
98 D. Yadav, S. Karki, M. B. Gohain and P. G. Ingole, *Chem. Eng. J.*, 2023, **472**, 144940.
99 S. Karki and P. G. Ingole, *Chem. Eng. J.*, 2022, **446**, 137303.
100 J. Robertson, *Mater. Sci. Eng., R*, 2002, **37**, 129–281.
101 X.-D. Pan, E. Maydell, R. Milne and D. Fabian, *Vacuum*, 1990, **41**, 1360–1363.
102 S. Karan, S. Samitsu, X. Peng, K. Kurashima and I. Ichinose, *Science*, 2012, **335**, 444–447.
103 J. Zhu, J. Hou, R. Zhang, S. Yuan, J. Li, M. Tian, P. Wang, Y. Zhang, A. Volodin and B. Van der Bruggen, *J. Mater. Chem. A*, 2018, **6**, 15701–15709.
104 W. B. Jensen, *J. Chem. Educ.*, 2006, **83**, 1283.
105 A. R. Madaria, A. Kumar, F. N. Ishikawa and C. Zhou, *Nano Res.*, 2010, **3**, 564–573.
106 K.-G. Zhou, K. Vasu, C. Cherian, M. Neek-Amal, J. C. Zhang, H. Ghorbanfekr-Kalashami, K. Huang, O. Marshall, V. Kravets and J. Abraham, *Nature*, 2018, **559**, 236–240.
107 B.-S. Kong, J. Geng and H.-T. Jung, *Chem. Commun.*, 2009, 2174–2176.
108 A. Achari, S. Sahana and M. Eswaramoorthy, *Energy Environ. Sci.*, 2016, **9**, 1224–1228.
109 D. Wang, Z. Wang, L. Wang, L. Hu and J. Jin, *Nanoscale*, 2015, **7**, 17649–17652.
110 S. Liu, R. Wang, M. Liu, J. Luo, X. Jin, J. Sun and L. Gao, *J. Mater. Chem. A*, 2014, **2**, 4598–4604.
111 X. Song, Y. Zhang, H. M. Abdel-Ghafar, E.-S. A. Abdel-Aal, M. Huang, S. Gul and H. Jiang, *Chem. Eng. J.*, 2021, **412**, 128607.
112 J.-J. Wang, H.-C. Yang, M.-B. Wu, X. Zhang and Z.-K. Xu, *J. Mater. Chem. A*, 2017, **5**, 16289–16295.
113 Y. Wen, X. Zhang, X. Li, Z. Wang and C. Y. Tang, *ACS Appl. Nano Mater.*, 2020, **3**, 9238–9248.
114 C.-Y. Zhu, H.-N. Li, J. Yang, J.-J. Li, J.-R. Ye and Z.-K. Xu, *J. Membr. Sci.*, 2020, **616**, 118557.
115 S. Wu, F. Wang, S. Zhou, L. Long, Z. Yang and C. Y. Tang, *Sep. Purif. Technol.*, 2022, **297**, 121547.
116 X.-H. Ma, Z.-K. Yao, Z. Yang, H. Guo, Z.-L. Xu, C. Y. Tang and M. Elimelech, *Environ. Sci. Technol. Lett.*, 2018, **5**, 123–130.
117 Z. Tan, S. Chen, X. Peng, L. Zhang and C. Gao, *Science*, 2018, **360**, 518–521.
118 Y. Ren, J. Zhu, S. Cong, J. Wang, B. Van der Bruggen, J. Liu and Y. Zhang, *J. Membr. Sci.*, 2019, **585**, 19–28.

119 B. Yuan, S. Zhao, P. Hu, J. Cui and Q. J. Niu, *Nat. Commun.*, 2020, **11**, 6102.
120 Z. Zhai, N. Zhao, W. Dong, P. Li, H. Sun and Q. J. Niu, *ACS Appl. Mater. Interfaces*, 2019, **11**, 12871–12879.
121 C. Li, S. Li, L. Tian, J. Zhang, B. Su and M. Z. Hu, *J. Membr. Sci.*, 2019, **572**, 520–531.
122 M. Hu and B. Mi, *Environ. Sci. Technol.*, 2013, **47**, 3715–3723.
123 Z. Yang, H. Guo, Z.-K. Yao, Y. Mei and C. Y. Tang, *Environ. Sci. Technol.*, 2019, **53**, 5301–5308.
124 L.-X. Dong, X.-C. Huang, Z. Wang, Z. Yang, X.-M. Wang and C. Y. Tang, *Sep. Purif. Technol.*, 2016, **166**, 230–239.
125 H. Zhang, X.-Y. Gong, W.-X. Li, X.-H. Ma, C. Y. Tang and Z.-L. Xu, *J. Membr. Sci.*, 2020, **616**, 118605.
126 J. Wang, Y. Wang, J. Zhu, Y. Zhang, J. Liu and B. Van der Bruggen, *J. Membr. Sci.*, 2017, **533**, 279–288.
127 S. Wang, Z. Yi, X. Zhao, Y. Zhou and C. Gao, *RSC Adv.*, 2017, **7**, 26136–26144.
128 W. Gai, Y. Zhang, Q. Zhao and T.-S. Chung, *J. Membr. Sci.*, 2021, **620**, 118952.
129 Y. Xu, W. Zhang, Z. Li, L. Shen, R. Li, M. Zhang, Y. Jiao, H. Lin and C. Y. Tang, *J. Mater. Chem. A*, 2022, **10**, 16430–16438.
130 F.-Y. Zhao, Q.-F. An, Y.-L. Ji and C.-J. Gao, *J. Membr. Sci.*, 2015, **492**, 412–421.
131 H. Shen, S. Wang, H. Xu, Y. Zhou and C. Gao, *J. Membr. Sci.*, 2018, **565**, 145–156.
132 Z. Yang, P.-F. Sun, X. Li, B. Gan, L. Wang, X. Song, H.-D. Park and C. Y. Tang, *Environ. Sci. Technol.*, 2020, **54**, 15563–15583.
133 X. Zhu, X. Cheng, X. Luo, Y. Liu, D. Xu, X. Tang, Z. Gan, L. Yang, G. Li and H. Liang, *Environ. Sci. Technol.*, 2020, **54**, 6365–6374.
134 G. M. Geise, D. R. Paul and B. D. Freeman, *Prog. Polym. Sci.*, 2014, **39**, 1–42.
135 L. E. Peng, Z. Yang, L. Long, S. Zhou, H. Guo and C. Y. Tang, *J. Membr. Sci.*, 2022, **641**, 119871.
136 H. Lonsdale, R. Riley, C. Lyons and D. Carosella Jr, *Membrane Processes in Industry and Biomedicine*, Plenum Press, 1971.
137 L. Long, C. Wu, Z. Yang and C. Y. Tang, *Environ. Sci. Technol.*, 2022, **56**, 2656–2664.
138 G. Z. Ramon, M. C. Wong and E. M. Hoek, *J. Membr. Sci.*, 2012, **415**, 298–305.
139 M. Kattula, K. Ponnuru, L. Zhu, W. Jia, H. Lin and E. P. Furlani, *Sci. Rep.*, 2015, **5**, 15016.
140 S. Shao, F. Zeng, L. Long, X. Zhu, L. E. Peng, F. Wang, Z. Yang and C. Y. Tang, *Environ. Sci. Technol.*, 2022, **56**, 12811–12827.
141 Q. Gan, C. Wu, L. Long, L. E. Peng, Z. Yang, H. Guo and C. Y. Tang, *Environ. Sci. Technol.*, 2023, **57**, 2548–2556.
142 Z. Yang, Y. Wu, H. Guo, X.-H. Ma, C.-E. Lin, Y. Zhou, B. Cao, B.-K. Zhu, K. Shih and C. Y. Tang, *J. Membr. Sci.*, 2017, **544**, 351–358.
143 J. Yuan, M. Wu, H. Wu, Y. Liu, X. You, R. Zhang, Y. Su, H. Yang, J. Shen and Z. Jiang, *J. Mater. Chem. A*, 2019, **7**, 25641–25649.
144 P.-F. Sun, P. Sarkar, E.-T. Yun, J. H. Lee, C. Y. Tang and H.-D. Park, *J. Membr. Sci.*, 2023, 121804.
145 G. Lai, W. Lau, P. Goh, Y. Tan, B. Ng and A. Ismail, *Arab. J. Chem.*, 2019, **12**, 75–87.
146 P.-F. Sun, Z. Yang, X. Song, J. H. Lee, C. Y. Tang and H.-D. Park, *Environ. Sci. Technol.*, 2021, **55**, 13219–13230.
147 D. Xu, X. Zhu, X. Luo, Y. Guo, Y. Liu, L. Yang, X. Tang, G. Li and H. Liang, *Environ. Sci. Technol.*, 2020, **55**, 1270–1278.
148 Z. Yang, Z.-w Zhou, H. Guo, Z. Yao, X.-h Ma, X. Song, S.-P. Feng and C. Y. Tang, *Environ. Sci. Technol.*, 2018, **52**, 9341–9349.
149 C. Jiang, L. Tian, Z. Zhai, Y. Shen, W. Dong, M. He, Y. Hou and Q. J. Niu, *J. Membr. Sci.*, 2019, **589**, 117244.
150 Z. Yang, F. Wang, H. Guo, L. E. Peng, X.-H. Ma, X.-X. Song, Z. Wang and C. Y. Tang, *Environ. Sci. Technol.*, 2020, **54**, 11611–11621.
151 G. Han, S. Zhang, X. Li, N. Widjojo and T.-S. Chung, *Chem. Eng. Sci.*, 2012, **80**, 219–231.
152 T. Wang, J. Wang, Z. Zhao, X. Zheng, J. Li, H. Liu and Z. Zhao, *Ind. Eng. Chem. Res.*, 2021, **60**, 14868–14883.
153 J. Liu, T. Huang, R. Ji, Z. Wang, C. Y. Tang and J. O. Leckie, *Environ. Sci. Technol.*, 2020, **54**, 12703–12712.
154 H. Guo, Y. Deng, Z. Tao, Z. Yao, J. Wang, C. Lin, T. Zhang, B. Zhu and C. Y. Tang, *Environ. Sci. Technol. Lett.*, 2016, **3**, 332–338.
155 H. Guo, Z. Yao, Z. Yang, X. Ma, J. Wang and C. Y. Tang, *Environ. Sci. Technol.*, 2017, **51**, 12638–12643.
156 H. Guo, Y. Deng, Z. Yao, Z. Yang, J. Wang, C. Lin, T. Zhang, B. Zhu and C. Y. Tang, *Water Res.*, 2017, **121**, 197–203.
157 K. A. Lundy and I. Cabasso, *Ind. Eng. Chem. Res.*, 1989, **28**, 742–756.
158 J. Lopez, S. Matson, J. Marchese and J. Quinn, *J. Membr. Sci.*, 1986, **27**, 301–325.
159 J. Wijmans and P. Hao, *J. Membr. Sci.*, 2015, **494**, 78–85.
160 B. Wu, N. Wang, J.-H. Lei, Y. Shen and Q.-F. An, *J. Membr. Sci.*, 2022, **643**, 120050.
161 X. Zhu, X. Zhang, J. Li, X. Luo, D. Xu, D. Wu, W. Wang, X. Cheng, G. Li and H. Liang, *J. Membr. Sci.*, 2021, **635**, 119536.
162 H. Lan, Y. Zhai, K. Chen, Z. Zhai, C. Jiang, P. Li, Y. Hou and Q. J. Niu, *Separ. Purif. Technol.*, 2022, **290**, 120781.
163 G. M. Geise, *Science*, 2021, **371**, 31–32.
164 T. E. Culp, B. Khara, K. P. Brickey, M. Geitner, T. J. Zimudzi, J. D. Wilbur, S. D. Jons, A. Roy, M. Paul and B. Ganapathysubramanian, *Science*, 2021, **371**, 72–75.
165 C. L. Ritt, J. R. Werber, M. Wang, Z. Yang, Y. Zhao, H. J. Kulik and M. Elimelech, *Proc. Natl. Acad. Sci. U. S. A.*, 2020, **117**, 30191–30200.
166 A. E. Childress and M. Elimelech, *Environ. Sci. Technol.*, 2000, **34**, 3710–3716.
167 J. Luo and Y. Wan, *J. Membr. Sci.*, 2013, **438**, 18–28.
168 R. Epsztein, E. Shaulsky, N. Dizge, D. M. Warsinger and M. Elimelech, *Environ. Sci. Technol.*, 2018, **52**, 4108–4116.
169 W. D. Mulhearn, V. P. Oleshko and C. M. Stafford, *J. Membr. Sci.*, 2021, **618**, 118637.
170 S.-J. Park, M.-S. Lee, M. E. Kilic, J. Ryu, H. Park, Y. I. Park, H. Kim, K.-R. Lee and J.-H. Lee, *Nano Lett.*, 2023, **23**, 4822–4829.

171 Q. Shen, Q. Song, Z. Mai, K.-R. Lee, T. Yoshioka, K. Guan, R. R. Gonzales and H. Matsuyama, *Sci. Adv.*, 2023, **9**, eadf6122.
172 Y. Gao, Y. Zhao, X.-M. Wang, C. Tang and X. Huang, *Environ. Sci. Technol.*, 2022, **56**, 14038–14047.
173 B. Gan, S. Qi, X. Song, Z. Yang, C. Y. Tang, X. Cao, Y. Zhou and C. Gao, *J. Membr. Sci.*, 2020, **612**, 118402.
174 S. Huang, J. Mansouri, P. Le-Clech, G. Leslie, C. Y. Tang and A. G. Fane, *J. Membr. Sci.*, 2022, **646**, 120248.
175 C. J. Porter, J. R. Werber, M. Zhong, C. J. Wilson and M. Elimelech, *ACS Nano*, 2020, **14**, 10894–10916.
176 H. Sui, B.-G. Han, J. K. Lee, P. Walian and B. K. Jap, *Nature*, 2001, **414**, 872–878.
177 M. Wang, Z. Wang, X. Wang, S. Wang, W. Ding and C. Gao, *Environ. Sci. Technol.*, 2015, **49**, 3761–3768.
178 J. K. Holt, H. G. Park, Y. Wang, M. Stadermann, A. B. Artyukhin, C. P. Grigoropoulos, A. Noy and O. Bakajin, *Science*, 2006, **312**, 1034–1037.
179 B. Corry, *J. Phys. Chem. B*, 2008, **112**, 1427–1434.
180 Y.-x Shen, W. Si, M. Erbakan, K. Decker, R. De Zorzi, P. O. Saboe, Y. J. Kang, S. Majd, P. J. Butler and T. Walz, *Proc. Natl. Acad. Sci. U. S. A.*, 2015, **112**, 9810–9815.
181 X.-B. Hu, Z. Chen, G. Tang, J.-L. Hou and Z.-T. Li, *J. Am. Chem. Soc.*, 2012, **134**, 8384–8387.
182 X. Zhou, G. Liu, K. Yamato, Y. Shen, R. Cheng, X. Wei, W. Bai, Y. Gao, H. Li and Y. Liu, *Nat. Commun.*, 2012, **3**, 949.
183 D. Cohen-Tanugi and J. C. Grossman, *Nano Lett.*, 2012, **12**, 3602–3608.
184 D. Cohen-Tanugi, L.-C. Lin and J. C. Grossman, *Nano Lett.*, 2016, **16**, 1027–1033.
185 S. Cong, Y. Yuan, J. Wang, Z. Wang, F. Kapteijn and X. Liu, *J. Am. Chem. Soc.*, 2021, **143**, 20055–20058.
186 C. Zhang, B.-H. Wu, M.-Q. Ma, Z. Wang and Z.-K. Xu, *Chem. Soc. Rev.*, 2019, **48**, 3811–3841.
187 L. Huang, M. Zhang, C. Li and G. Shi, *J. Phys. Chem. Lett.*, 2015, **6**, 2806–2815.
188 M. M. Pendergast and E. M. Hoek, *Energy Environ. Sci.*, 2011, **4**, 1946–1971.
189 Z. Yang, X.-H. Ma and C. Y. Tang, *Desalination*, 2018, **434**, 37–59.
190 H. Guo, R. Dai, M. Xie, L. E. Peng, Z. Yao, Z. Yang, L. D. Nghiem, S. A. Snyder, Z. Wang and C. Y. Tang, *Environ. Sci. Technol. Lett.*, 2022, **9**, 247–257.
191 J. Kang, Y. Ko, J. P. Kim, J. Y. Kim, J. Kim, O. Kwon, K. C. Kim and D. W. Kim, *Nat. Commun.*, 2023, **14**, 901.
192 P. Marchetti, M. F. Jimenez Solomon, G. Szekely and A. G. Livingston, *Chem. Rev.*, 2014, **114**, 10735–10806.
193 G. M. Shi, Y. Feng, B. Li, H. M. Tham, J.-Y. Lai and T.-S. Chung, *Prog. Polym. Sci.*, 2021, **123**, 101470.
194 Z. Jiang, R. Dong, A. M. Evans, N. Biere, M. A. Ebrahim, S. Li, D. Anselmetti, W. R. Dichtel and A. G. Livingston, *Nature*, 2022, **609**, 58–64.
195 S. Li, R. Dong, V.-E. Musteata, J. Kim, N. D. Rangnekar, J. Johnson, B. D. Marshall, S. Chisca, J. Xu and S. Hoy, *Science*, 2022, **377**, 1555–1561.
196 M. F. Jimenez-Solomon, Q. Song, K. E. Jelfs, M. Munoz-Ibanez and A. G. Livingston, *Nat. Mater.*, 2016, **15**, 760–767.
197 R. S. K. Valappil, N. Ghasem and M. Al-Marzouqi, *J. Ind. Eng. Chem.*, 2021, **98**, 103–129.
198 T. Zhu, Q. Xia, J. Zuo, S. Liu, X. Yu and Y. Wang, *Adv. Membr.*, 2021, **1**, 100008.
199 F. Wiesler and R. Sodaro, *Ultrapure Water*, 1996, **13**, 53–56.
200 Y. Zhao, N. Li, J. Shi, Y. Xia, B. Zhu, R. Shao, C. Min, Z. Xu and H. Deng, *Sep. Purif. Technol.*, 2022, **286**, 120419.
201 J. R. McCutcheon and M. S. Mauter, *Science*, 2023, **380**, 242–244.